INTERPLANETARY TRAJECTORY ANALYSIS USING INVARIANT MANIFOLDS

A Project

Presented to

The Faculty of the Department of Aerospace Engineering

San José State University

In Partial Fulfillment

of the Requirements for the Degree

Master of Science

by

Jazmine Eubanks

May 2021

The Designated Project Advisor Approves the Project Titled

INTERPLANETARY TRAJECTORY ANALYSIS USING INVARIANT MANIFOLDS

by

Jazmine Eubanks

APPROVED FOR THE DEPARTMENT OF AEROSPACE ENGINEERING

SAN JOSÉ STATE UNIVERSITY

May 2021

Dr. Lucia Capdevila	Department of Aerospace Engineering	Advisor

ABSTRACT

INTERPLANETARY TRAJECTORY ANALYSIS
USING
INVARIANT MANIFOLDS

by Jazmine Eubanks

The purpose of this project is to study the dynamics of low energy interplanetary trajectories starting in the Earth-Moon system, with the potential to reach Mars. The intended methodology to study these low energy trajectories involve calculating periodic orbits in the Earth-Moon system and the invariant manifolds associated with these orbits, then expanding them to become interplanetary trajectories. Potential applications of these low energy trajectories can be applied to sending satellites to a Martian orbit from Earth using minimal changes in velocity. This project will explore the viability of achieving an interplanetary trajectory using manifolds.

I'd like to dedicate this work to my loving parents Sony and Phillip Eubanks, who have supported me throughout this entire journey, through the happy times and hard times. I love you both dearly, and I wouldn't have been able to complete this work without you.

ACKNOWLEDGEMENTS

I'd like to thank Dr. Lucia Capdevila for the tireless time and energy she spent on me helping me produce this work. Special thanks to Robert Pritchett for his guidance. I'd also like to send a special thanks to Romalyn Mirador and Dhathri Somavarapu for their time and support through the project. Thank you Marta Ramirez-Rodenas and Dr. Nikos Mourtos. Last but not least, I'd like to thank my coworkers at Maxar Technologies for their support and encouragement. Thank you all so much for your time and support and helping me get through the Masters degree, I am forever grateful.

TABLE OF CONTENTS

CHAPTER

Nomenclature **ix**

Abbreviations **xi**

List of Tables **xii**

List of Figures **xiii**

1 INTRODUCTION 1

1.1 Motivation 1

1.2 Literature Review 1

1.3 Current Project 8

1.4 Methodology 9

2 EQUATIONS OF MOTION 10

2.1 Dynamics of the Circular Restricted Three-Body Problem 10

2.1.1 Derivation of Equations of Motion 10

2.1.2 Derivation of Effective Potential 14

2.2 Characteristic Parameters 15

2.3 Libration Points 16

2.4 Coordinate Transformation 17

2.5 Jacobi Constant 21

3 GENERATING PERIODIC ORBITS 23

3.1 State Transition Matrix 23

3.1.1 Verifying the State Transition Matrix 25

3.2 Differential Corrector 26

3.3 Periodic Orbits 26

4 INVARIANT MANIFOLDS 31

4.1 Manifold Theory of fixed points 31

4.1.1 Eigenvalues 34

4.2 Methodology to Calculate Invariant Manifolds 34

4.2.1 Calculating the Stable Manifolds 36

4.2.2 Calculating the Unstable Manifolds 37

4.2.3 Verifying the manifolds 37

4.2.4 Finding a feasible trajectory 43

5 ANALYSIS OF TRAJECTORIES AND RESULTS 46

5.1 Viable Orbits 46

6 CONCLUSION 49

6.1 Future Work 49

REFERENCES 51

NOMENCLATURE

$\vec{a}$	acceleration vector
A_t	inertial to rotating frame transformation vector
C	Jacobi constant
$\vec{F}$	force vector
G	gravitational constant
l^*	characteristic length
m	mass of particle
μ	mass ratio
m_1	larger primary mass
m_2	smaller primary mass
P	particle
${}^R\vec{r}^P$	position of particle with respect to the rotating frame
r_1	distance from particle from planetary body of m_1
r_2	distance from particle from planetary body of m_2
t^*	characteristic time
$\dot{\vec{\theta}}$	instantaneous angular velocity
U	pseudo-potential
$\vec{v}$	velocity vector
${}^I\vec{w}^R$	angular velocity in the rotating frame
${}^R\vec{w}^{BF}$	angular velocity in the body frame
x	x position in the rotating frame
X	x position in the inertial frame

y	y position in the rotating frame
Y	y position in the inertial frame
z	z position in the rotating frame
Z	z position in the inertial frame

ABBREVIATIONS

$CR3BP$	Circular Restricted Three-Body Problem
EOM	Equations of Motion
IPS	Inter-Planetary Superhighway
$P3DRO$	Period 3 Distant Retrograde Orbits
$RTBP$	Restricted Three Body Problem
SOI	Sphere of Influence
STM	State Transition Matrix
WSB	Weak Stability Boundary

LIST OF TABLES

Table

2.1 Parameters in the Earth-Moon system 16

2.2 Location of the libration points in the Earth-Moon system 17

LIST OF FIGURES

Figure

1.2.1 Metro Map displaying current work on low energy trajectories in the Solar System 5

2.1.1 Visualization of the CR3BP 11

2.3.1 Location of libration points in the Earth-Moon system 18

2.4.1 Rotation transformation 19

2.5.1 Jacobi constant of an orbit around L_1 in the Earth-Moon system . . . 22

3.3.1 Initial guess for L_1 Lyapunov orbit in Earth-Moon system 28

3.3.2 Lyapunov periodic orbit about L_1 in Earth-Moon system 29

3.3.3 P3DRO periodic orbit 30

4.2.1 Flowchart for detecting crashing manifold trajectories 35

4.2.2 Stable Lyapunov manifolds 38

4.2.3 Stable P3DRO manifolds 39

4.2.4 Unstable Lyapunov manifolds 40

4.2.5 Unstable P3DRO manifolds 41

4.2.6 Verifying unstable manifolds converge into periodic orbit 42

4.2.7 Trajectories intersecting with the Earth 44

4.2.8 Trajectories intersecting with the Moon 45

5.1.1 Potential viable trajectory to Mars in the rotating frame 48

CHAPTER 1

INTRODUCTION

1.1 Motivation

The study of low energy transfers can become very useful for sending supplies to a Lunar or a Martian base. These low energy transfers may take a long time, but could potentially use less propellant than a Hohmann Transfer orbit, expanding the capacity in the spacecraft for additional cargo or supplies [1]. Currently, there is some research in optimizing low energy transfers between libration points L_1 and L_2, but limited research on interplanetary transfers between multiple planetary bodies. Topputo et al. exploits a patched conics path, using a series of three-body problems to refine an interplanetary trajectory [2]. This project will be researching the beginning methods to refine a path for an interplanetary trajectory using the Circular Restricted Three-Body Problem (CR3BP), and will set up a foundation to study multi-planetary trajectories in the future, by determining where the trajectories propagate within the solar system.

1.2 Literature Review

Koon et al. discuss the heteroclinic connections between the Lagrangian points in applications using low energy transfer orbits and to explain the dynamics of asteroids and comets [1]. Koon et al. describe the transition in resonance of comet orbits while outside of Jupiter's sphere of influence, and inside the orbit of

Jupiter [1]. Koon et al. note that resonance transitions of the comets of Jupiter follow the invariant manifolds associated with Lagrangian points L_1 and L_2 [1]. There exists homoclinic orbits and heteroclinic trajectories about L_1 and L_2. Homoclinic orbits asymptotically approach Lyapunov periodic orbits, and heteroclinic trajectories are orbits connecting intersections of stable and unstable manifolds of two different periodic Lyapunov orbits [1]. By demonstrating a heteroclinic connection, it is possible to predict a temporary transition orbit. The findings of Koon et al. can be used to design multi-planetary space missions, or missions from planets to their outer moons, including between the Earth and Moon [1]. Koon et al. focuses on using the Hamiltonian structure by using the covariance of the Lagrangian formulation and using the coordinates in a moving frame. Using this method provides the Lagrangian form and the Hamiltonian form given by the Lengendre transformation, though Koon et al. also derives the equations of motion using Newton's method [1].

Cox et al. added low thrust in the CR3BP, which use the Hamiltonian approach to derive the equations of motion. Cox et al. also develops an energy plane, which is defined as the low thrust arc that lies fixed in an Earth-Moon rotating frame. By using the Hamiltonian values in the energy plane, Cox et al. were able to manipulate the forbidden regions about L_1 and L_2 [3]. Between the forbidden regions, there is an opening at L_1 and L_2, called gateways. The lower energy trajectories cannot pass through the L_1 gateway and stay within the interior region of the planetary orbit. The trajectories within a specified energy set have just enough energy to pass through the L_1 gateway but does not have enough energy to pass through the L_2 gateway. A small percentage of these trajectories will not pass through the L_1 gateway, even though the trajectories have sufficient energy, verifying that passage through L_1 is not guaranteed. The high energy trajectories

pass through both the L_1 and the L_2 gateway, though it's not guaranteed that these trajectories will pass through the L_2 gateway [3].

Topputo et al. solved for a four-body problem describing interplanetary transfers using two coupled three-body problems, such as the Sun-Earth and Sun-Jupiter systems, and various other Sun-planet systems [2]. Topputo et al. used a linear approximation to calculate the manifolds of the Lyapunov orbit before intersecting the stable and unstable manifolds to determine the optimal interplanetary trajectory [2]. Topputo et al. calculated the departure and arrival candidate trajectories from the generated manifolds of the Earth-Jupiter transfer [2]. By using Poincaré sections, Topputo et al. were able to search for an optimal transfer orbit between Earth and Jupiter [2]. According to Topputo et al., the method of intersecting departure manifolds from Earth and arrival manifolds from Jupiter works for travel to outer planets in the solar system, or outer planets and their respective moons, though travel to the Lyapunov periodic orbits near the inner planets such as Earth, Venus, and Mars, is more difficult due to the departure and arrival manifolds rarely intersecting. To remedy this situation, Topputo et al. added an intermediary arc to connect the arrival and departure manifolds. Even though manifolds of periodic orbits about inner planets do not intersect often, outer planets and systems involving planets and their moons often have intersecting manifolds [2].

Heiligers et al. takes a different approach and investigates solar sail transfers between multiple three-body problems [4]. The time-optimal transfer is sought by using a direct pseudospectral method, and is a constraint on the attitude of the solar sails. Although the current work will not be accounting for external thrusts generated by the solar sail, Heiligers et al. accounts for perturbations of the planets outside of the three-body problem in focus, and interestingly takes a "two-phase approach" and creates a linkage trajectory, or a connection between Earth L_2 halo

orbit and Mars L_1 halo orbit [4].

Vaquero studied unstable resonant orbits between multi-body systems. A multi-dimensional Newton-Raphson differential corrections process, also known as the multiple shooting algorithm, was used to connect a series of patch points, the estimated positions, together to create a continuous trajectory and allow more control over the trajectory by applying constraints [5]. Vaquero used the multiple shooting algorithms to create a continuous multi-body transfer trajectory from the initial state, calculated using differential corrections with information from the State Transition Matrix [5].

Based on the research and ideas to develop a solar system superhighway by Lo [6], a metro map was developed to visually express the current work completed for mostly low thrust trajectories within the solar system, similar to the metro map representation in Dynamical Systems, the Three-Body Problem and Space Mission Design [1]. Current work is completed extensively in the Earth-Moon system, where this project will start developing the equations of motion and initial manifolds. The metro map displayed in Figure 1.2.1 is a visual representation of researched trajectories through the solar system using low thrust.

BepiColumbo is a dual spacecraft mission to Mercury on a journey that takes approximately six years, using multiple gravity assist and solar electric propulsion (SEP) thrust arcs [7]. The arrival approach implements a gravitational capture using the Sun's gravity to weakly capture the spacecraft in the Sun-Mercury system [7]. The spacecraft then reaches a Mercury Orbit Insertion (MOI), placing the spacecraft into a 400km by 1200km polar orbit [7].

Finocchietti et al. have also taken up the idea of the interplanetary superhighway (IPS), and mentioned inner planets do not intersect and that pure low energy IPS transfers without the use of thrusters cannot be used [8].

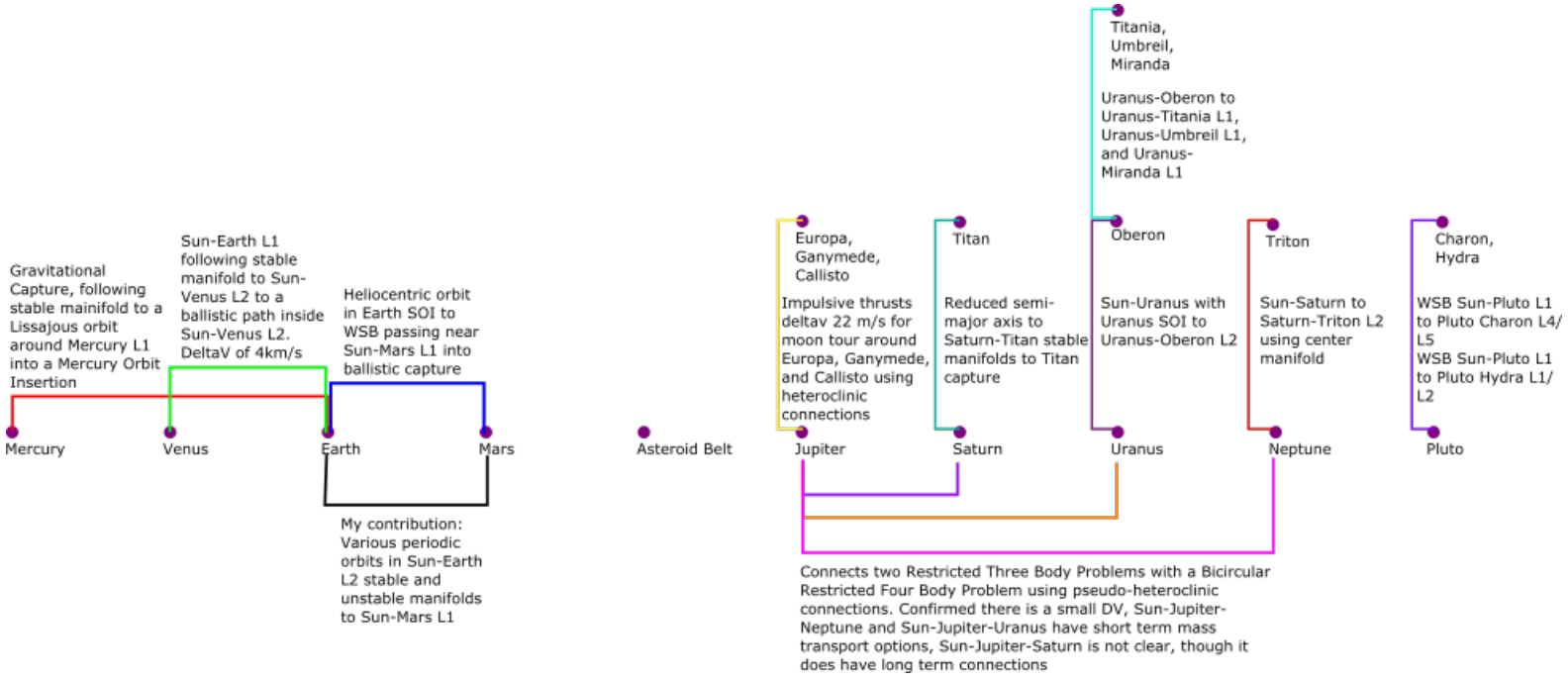

Figure 1.2.1: Metro Map displaying current work on low energy trajectories in the Solar System

The transfer to Venus includes a minimal number of ballistic phases [8]. Starting from a Geostationary Transfer Orbit (GTO), in the Sun-Earth L_1 system, Finocchietti et al. followed the stable manifold of the Sun-Venus L_2 to a ballistic path inside the Sun-Venus L_2 [8].

Kakoi attempts to find a manifold connecting the Sun-Earth and the Sun-Mars system using various methodologies [9]. Blending the CR3BP into a four-body problem has limitations in the level of accuracy due to the fact that the Mars' orbit is more eccentric than Earth's and the Moon's orbit, therefore a five-body problem must be used [9]. The complex five body problem is constructed by using an ephemeris state of the destination planet blended with the Sun-Earth-Moon system [9]. The trajectory was calculated without taking into account Mars' gravity since the gravitational force is small [9]. Kakoi investigated multiple transfer scenarios, including Sun-Earth manifold transfers, Earth-Moon manifold transfers, and direct transfers [9], but the models were not optimized without use of ΔV.

Topputo and Belbruno constructed weak stability boundary (WSB), or a ballistic capture transfer, from a heliocentric orbit in Earth's sphere of influence (SOI) to pass near Sun-Mars L_1 ending a ballistic capture around Mars [10]. Using ideas from Hiten, Belbruno [11] used a ballistic capture from Earth to the Moon, Topputo and Belbruno investigated if a ballistic capture can be used to find a trajectory that enters into a ballistic capture around Mars [10]. In the sample solution Topputo et al. the trajectory orbits Mars approximately 6 times before being pulled into a ballistic capture [10]. While there is a ΔV required, compared to a Hohmann transfer, there is a 4-18% savings using a WSB [10].

Koon et al. found a trajectory touring the moons of Jupiter. The touring of the moons involves making orbits around each moon for a duration of time before continuing to the next planetary body, unlike Voyager's missions which were flybys

[1]. The trajectory uses impulsive thrusts with a ΔV of $22m/s$ for a tour around Europa, Ganymede, and Callisto using heteroclinic connections. Barrabés et al. constructed trajectories connecting Jupiter, Saturn, Uranus, and Neptune by connecting two Restricted Three Body Problems (RTBP) using pseudo-heteroclinic connections, with a small ΔV [12]. The Sun-Jupiter-Neptune and Sun-Jupiter-Uranus systems have short term mass transport options between those two systems, yet the Sun-Jupiter-Uranus and the Sun-Jupiter-Saturn systems do not have clear intersections for short term transports, yet some longer term timeframes were not tested, but seem optimal to improve connections between systems [12].

Bosanac et al. investigate trajectory design using invariant manifolds and resonant gravity assists between Saturn and Titan [13]. They use stable manifolds into a capture around Titan, and discover the ΔV for gravity assists and capture vary based on the Jacobi constant, but the time of flight decreases as the Jacobi constant decreases. [13]. The trajectory with the Jacobi of $C = 3.008$ has a total ΔV of $626.2m/s$, the trajectory with the Jacobi of $C = 3.010$ has a total ΔV of $654.4m/s$, and the trajectory with the Jacobi of $C = 3.012$ has a total ΔV of $645.7m/s$, displaying that the ΔV is not dependent on the Jacobi constant [13].

Pergola et al. investigated the possibility of interplanetary transfer around Uranus and its moons [14]. Starting at the Sun-Uranus system with Uranus SOI, the trajectory ballistically follows the stable manifold to L_2 in the Uranus-Oberon system, then ballistically follows the stable manifolds to Uranus-Titania L_1, and Uranus-Miranda L_1 [14]. The transfer from the Sun-Uranus system to Uranus-Oberon L_2 has a ΔV of $17.56km/s$, and the transfer from Uranus-Oberon L_2 to Uranus-Titania L_1 has a ΔV of $2.26km/s$ [14].

Stuchi et al. finds trajectories from the Sun-Neptune following a center manifold on a Lyapunov orbit into Neptune-Triton L_2 [15]. Some of the different

constraints faced in this Planet-Moon system unlike the other systems is the fact that Neptune is oblate and highly inclined, and Triton is in a retrograde orbit around Neptune [15].

Liang et al. studies the effects of L_4 and L_5 on low energy WSB transfers from the Sun-Pluto system to Pluto-Moon systems where, Hydra is treated as a contact binary system due to its irregular shape [16]. The WSB is calculated between multiple trajectories on the Lyapunov orbit including Sun-Pluto L_1 and Pluto-Charon L_5, and Sun-Pluto L_1 and Pluto-Charon L_4 [16]. One of the calculated trajectories towards Hydra starts at a $200km$ parking orbit and include three patch points [16]. The first patch point is between the parking orbit and Sun-Pluto L_1 using a ΔV of $125.75m/s$, the second patch point is between the Sun-Pluto L_1 and Pluto-Hydra L_2 uses a ΔV of $16.29m/s$, and the third patch point is between Pluto-Hydra L_2 and a Hydra capture, with a ΔV of $22.84m/s$ [16]. Liang et al. also studies the trajectories to the Hydra contact binary libration points [16].

Using all of the previous literature as a guide to determine the gaps to contribute to the IPS, this paper will explore the use of a different type of orbit, the Period-Three Distant Retrograde Orbit (P3DRO) instead of the common Lyapunov and halo orbits used in previous literature.

1.3 Current Project

This project will analyze trajectories in the Earth-Moon rotating frame by calculating the invariant manifolds associated with periodic orbits in the CR3BP. By generating a periodic orbit in the rotating reference frame and propagating the trajectories on the manifolds associated with different positions on the periodic orbit, it is possible to determine where the trajectories propagate in the solar

system. Firstly, the equations of motion and initial manifolds are generated in the Earth-Moon system using a Lyapunov orbit, to ensure the accuracy of the propagation. Next, the manifolds associated with an Earth-Moon P3DRO are calculated and evaluated as potential transfer trajectories to the Sun-Mars system.

1.4 Methodology

The CR3BP system includes two bodies, in this case the Earth-Moon system, containing multiple solutions and infinite number of periodic orbits, where each periodic orbit is associated with invariant manifolds. To start, the equations of motion are derived and linearized, the Earth-Moon mass ratios are calculated, including the characteristic parameters: mass, length, and time values in the Earth-Moon system, and the location of the libration points L_1-L_5 are calculated. The Jacobi Constant is utilized to verify the equations of motion. From the linearized equations of motion, the state transition matrix elements are defined, and implemented in a shooting method to generate Lyapunov periodic orbits about one of the libration points, the equilibrium solutions of the CR3BP. The Monodromy Matrix is generated to analyze the dynamical stability of the orbit, and is used to propagate the trajectories on the invariant manifolds. Once the manifolds are generated, the trajectories residing on the manifolds are propagated to see the path traced in the solar system. The manifolds are generated in P3DRO orbits around Earth-Moon L_1.

CHAPTER 2

EQUATIONS OF MOTION

2.1 Dynamics of the Circular Restricted Three-Body Problem

Koon et al. suggests starting with the planar CR3BP to estimate an appropriate starting model [1]. The use of the planar CR3BP is ideal for problems where the bodies of interest are mostly under the gravitational force of one planetary body, such as the Sun. There are multiple ways to derive the equations of motion, and this paper will derive the equations of motion using Newton's method, similarly to Koon et al. [1].

To develop the equations of motion for a particle, P in reference to two planetary bodies, m_1, and m_2, represent the larger and smaller primary masses respectively. Start with Newton's equations, $\vec{F} = m\vec{a}$, or $\vec{F} = \frac{d}{dt}m\vec{v}$, where m is the mass of the particle, $\vec{a}$ is the acceleration vector of the particle, and $\vec{v}$ is the velocity vector of the particle. To differentiate between vectors and scalars, vectors are defined with a vector symbol, and scalars are italicized.

2.1.1 Derivation of Equations of Motion

Traditionally there are three main ways to approach the equations of motion, the Newtonian, Lagrangian, and the Hamiltonian approach. Here, the Newton approach is used to derive the equations of motion as visualized in Figure 2.1.1.

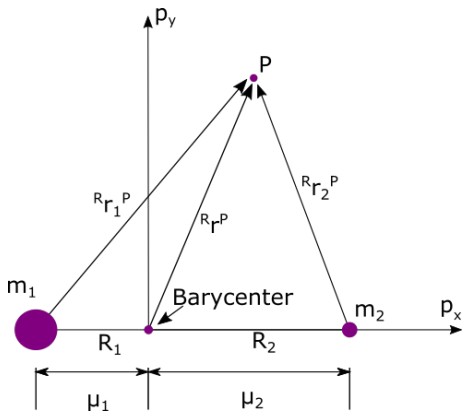

Figure 2.1.1: Visualization of the CR3BP

While deriving the equations of motion, the following assumptions are made: the m_1 is much larger than m_2, which is much larger than the negligible mass of the spacecraft, all the masses are considered point masses, gravity is the only force acting on the bodies, and the primary masses are orbiting about a barycenter in the rotating frame. Knowing Newton's equation, $\vec{F} = m\vec{a}$, derive the acceleration vector starting with position and angular velocity:

$$^{R}\vec{r}^{P} = x\vec{p_x} + y\vec{p_y} + z\vec{p_z} \tag{2.1.1}$$

$$^{R}\vec{w}^{BF} = 1\vec{p_z} \tag{2.1.2}$$

Since the problem is defined in the rotating frame, it is easier to define it in dimensionless terms, so all parameters in Equations (2.1.1) and (2.1.2) are non-dimensional [17].

Deriving the velocity from the position and angular velocity, equations 2.1.1 and 2.1.2:

$$ {}^{R}\vec{v}^{P} = {}^{PF}\frac{d}{dt}{}^{R}\vec{r}^{P} + {}^{R}\vec{w}^{BF} \times {}^{R}\vec{r}^{P} \tag{2.1.3} $$

$$ = [\dot{x}\vec{p_x} + \dot{y}\vec{p_y} + \dot{z}\vec{p_z}] + 1\vec{p_z} \times [x\vec{p_x} + y\vec{p_y} + z\vec{p_z}] \tag{2.1.4} $$

$$ = (\dot{x} - y)\vec{p_x} + (\dot{y} + x)\vec{p_y} + (\dot{z})\vec{p_z}] \tag{2.1.5} $$

Deriving the acceleration from the velocity and angular velocity, equations 2.1.2 and 2.1.5:

$$ {}^{R}\vec{a}^{P} = {}^{PF}\frac{d}{dt}{}^{R}\vec{v}^{P} + {}^{R}\vec{w}^{BF} \times {}^{R}\vec{v}^{P} \tag{2.1.6} $$

$$ = [(\ddot{x} - \dot{y})\vec{p_x} + (\ddot{y} + \dot{x})\vec{p_y} + \ddot{z}\vec{p_z}] + 1\vec{p_z} \times [(\dot{x} - y)\vec{p_x} + (\dot{(y)} + x)\vec{p_y} + (\dot{z})\vec{p_z}] \tag{2.1.7} $$

$$ = (\ddot{x} - 2\dot{y} - x)\vec{p_x} + (\ddot{y} + 2\dot{x} - y)\vec{p_y} + (\ddot{z})\vec{p_z}] \tag{2.1.8} $$

Now the acceleration is derived from Newton's approach. To derive the force from Newton's method:

$$ -\frac{Gmm_1{}^{R}r_1^{P}}{r_1^3} - \frac{Gmm_2{}^{R}r_2^{P}}{r_2^3} = m{}^{R}a^{P} \tag{2.1.9} $$

$$ -\frac{Gmm_1{}^{R}r_1^{P}}{\|{}^{R}r_1^{P}\|}\frac{{}^{R}r_1^{P}}{\|{}^{R}r_1^{P}\|} - \frac{Gmm_2{}^{R}r_2^{P}}{\|{}^{R}r_2^{P}\|^2}\frac{{}^{R}r_2^{P}}{\|{}^{R}r_2^{P}\|} \tag{2.1.10} $$

where

$$ {}^{R}r_1^P = {}^{R}r^P + \mu_2\vec{p_x} \tag{2.1.11} $$

$$ {}^{R}r_1^P = (x+\mu_2)\vec{p_x} + y\vec{p_y} + z\vec{p_z} \tag{2.1.12} $$

$$ r_1 = \|{}^{R}r_1^P\| = \sqrt{(x+\mu_2)\vec{p_x} + y\vec{p_y} + z\vec{p_z}} \tag{2.1.13} $$

$$ {}^{R}r_2^P = {}^{R}r^P - \mu_1\vec{p_x} \tag{2.1.14} $$

$$ {}^{R}r_2^P = (x-\mu_1)\vec{p_x} + y\vec{p_y} + z\vec{p_z} \tag{2.1.15} $$

$$ r_2 = \|{}^{R}r_2^P\| = \sqrt{(x-\mu_1)\vec{p_x} + y\vec{p_y} + z\vec{p_z}} \tag{2.1.16} $$

$$ \frac{1}{m}(-\frac{Gmm_1{}^{R}r_1^P}{r_1^3} - \frac{Gmm_2{}^{R}r_2^P}{r_2^3}) = {}^{R}a^P \tag{2.1.17} $$

$$ -\frac{\mu_1[(x+\mu_2)\vec{p_x} + y\vec{p_y} + z\vec{p_z}]}{[(x+\mu_2)^2+y^2+z^2]^{\frac{3}{2}}} - \frac{\mu_2[(x-\mu_1)\vec{p_x} + y\vec{p_y} + z\vec{p_z}]}{[(x-\mu_1)^2+y^2+z^2]^{\frac{3}{2}}} = \tag{2.1.18} $$

where μ is the mass ratio, $\mu_2 = \mu, \mu_1 = 1-\mu, \mu_1+\mu_2 = 1$. Combining the derived acceleration, equation 2.1.8, and the derived force, equation 2.1.18:

$$ -\frac{\mu_1[(x+\mu_2)\vec{p_x} + y\vec{p_y} + z\vec{p_z}]}{[(x+\mu_2)^2+y^2+z^2]^{\frac{3}{2}}} - \frac{\mu_2[(x-\mu_1)\vec{p_x} + y\vec{p_y} + z\vec{p_z}]}{[(x-\mu_1)^2+y^2+z^2]^{\frac{3}{2}}} = \tag{2.1.19} $$

$$ (\ddot{x} - 2\dot{y} - x)\vec{p_x} + (\ddot{y} + 2\dot{x} - y)\vec{p_y} + (\ddot{z})\vec{p_z} \tag{2.1.20} $$

Collecting coefficients:

$$ \vec{p_x} : -\frac{\mu_1(x+\mu_2)}{[(x+\mu_2)^2+y^2+z^2]^{\frac{3}{2}}} - \frac{\mu_2(x-\mu_1)}{[(x-\mu_1)^2+y^2+z^2]^{\frac{3}{2}}} = \ddot{x} - 2\dot{y} - x \tag{2.1.21} $$

$$ \vec{p_y} : -\frac{\mu_1 y}{[(x+\mu_2)^2+y^2+z^2]^{\frac{3}{2}}} - \frac{\mu_2 y}{[(x-\mu_1)^2+y^2+z^2]^{\frac{3}{2}}} = \ddot{y} + 2\dot{x} - y \tag{2.1.22} $$

$$ \vec{p_z} : -\frac{\mu_1 z}{[(x+\mu_2)^2+y^2+z^2]^{\frac{3}{2}}} - \frac{\mu_2 z}{[(x-\mu_1)^2+y^2+z^2]^{\frac{3}{2}}} = \ddot{z} \tag{2.1.23} $$

Substituting in equations 2.1.13 and 2.1.16, the equations of motion are defined as

$$\vec{p_x} : x - \frac{\mu_1(x+\mu_2)}{r_1^3} - \frac{\mu_2(x-\mu_1)}{r_2^3} = \ddot{x} - 2\dot{y} \tag{2.1.24}$$

$$\vec{p_y} : y - \frac{\mu_1 y}{r_1^3} - \frac{\mu_2 y}{r_2^3} = \ddot{y} + 2\dot{x} \tag{2.1.25}$$

$$\vec{p_z} : -\frac{\mu_1 z}{r_1^3} - \frac{\mu_2 z}{r_2^3} = \ddot{z} \tag{2.1.26}$$

2.1.2 Derivation of Effective Potential

To determine the effective potential, integrate the left hand side of the equations of motion:

$$U = \frac{x^2+y^2}{2} + \frac{\mu_1}{r_1} + \frac{\mu_2}{r_2} \tag{2.1.27}$$

Using chain rule, where $(x+\mu_2)^2 + y^2 + z^2 = e_1$, $\frac{\partial}{\partial e}\frac{1}{e^{1/2}}\frac{\partial e}{\partial x}$ where $\frac{\partial}{\partial e}\frac{1}{e^{1/2}} = -\frac{1}{2e^{3/2}}$ and $\frac{\partial e}{\partial x} = \frac{\partial}{\partial x}(x+\mu_2)^2 + y^2 + z^2 = 2(x+\mu_2)$. Applying the same rules for the x,y,z derivatives are now equal to the left hand side:

$$U_x : \frac{\partial U}{\partial x} = x - \frac{\mu_1(x+\mu_2)}{r_1} - \frac{\mu_2(x-\mu_1)}{r_2} \tag{2.1.28}$$

$$U_y : \frac{\partial U}{\partial y} = y - \frac{\mu_1 y}{r_1} - \frac{\mu_2 y}{r_2} \tag{2.1.29}$$

$$U_z : \frac{\partial U}{\partial z} = -\frac{\mu_1 z}{r_1} - \frac{\mu_2 z}{r_2} \tag{2.1.30}$$

We can solve for the second derivative of the effective potential

$$U_x = x - \frac{\mu_1(x+\mu_2)}{r_1} - \frac{\mu_2(x-\mu_1)}{r_2} = x - \frac{\mu_1 x + \mu_1\mu_2}{r_1} - \frac{\mu_2 x - \mu_1\mu_2}{r_2} \tag{2.1.31}$$

$$U_{xx} = -\left[\frac{\mu_1}{r_1} - \frac{\mu_1(x+\mu_2)^2}{r_1^3}\right] - \left[\frac{\mu_2}{r_2} - \frac{\mu_2(x-\mu_1)^2}{r_2^3}\right] \tag{2.1.32}$$

$$U_{xy} = \frac{y\mu_1(x+\mu_2)}{r_1^3} - \frac{y\mu_2(x-\mu_1)}{r_2^3} = U_{yx} \tag{2.1.33}$$

$$U_{xz} = \frac{z\mu_1(x+\mu_2)}{r_1^3} - \frac{z\mu_2(x-\mu_1)}{r_2^3} = U_{zx} \tag{2.1.34}$$

$$U_y = y - \frac{\mu_1 y}{r_1} - \frac{\mu_2 y}{r_2} \tag{2.1.35}$$

$$U_{yx} = \frac{y\mu_1(x+\mu_2)}{r_1^3} - \frac{y\mu_2(x-\mu_1)}{r_2^3} = U_{xy} \tag{2.1.36}$$

$$U_{yy} = -\left[\frac{\mu_1}{r_1} - \frac{\mu_1 y^2}{r_1^3}\right] - \left[\frac{\mu_2}{r_2} - \frac{\mu_2 y^2}{r_2^3}\right] \tag{2.1.37}$$

$$U_{yz} = \frac{yz\mu_1}{r_1^3} - \frac{yz\mu_2}{r_2^3} = U_{zy} \tag{2.1.38}$$

$$U_z = z - \frac{\mu_1 z}{r_1} - \frac{\mu_2 z}{r_2} \tag{2.1.39}$$

$$U_{zx} = \frac{z\mu_1(x+\mu_2)}{r_1^3} - \frac{z\mu_2(x-\mu_1)}{r_2^3} = U_{xz} \tag{2.1.40}$$

$$U_{zy} = \frac{yz\mu_1}{r_1^3} - \frac{yz\mu_2}{r_2^3} = U_{yz} \tag{2.1.41}$$

$$U_{zz} = -\left[\frac{\mu_1}{r_1} - \frac{\mu_1 z^2}{r_1^3}\right] - \left[\frac{\mu_2}{r_2} - \frac{\mu_2 z^2}{r_2^3}\right] \tag{2.1.42}$$

2.2 Characteristic Parameters

Three characteristic parameters must be defined: the characteristic length, l^*, the characteristic mass M, and the characteristic time t^*. The characteristic length is defined as the distance between the two primary masses in the CR3BP, in this case, the Earth and the Moon. The characteristic mass is defined as the sum of the

two masses, and characteristic time is the dimensionless time value in the system. The characteristic length is average distance between two planetary bodies, the characteristic mass is calculated from $m_1 + m_2$, and characteristic time is calculated from $\sqrt{l^{*3}/G(m_1 + m_2)}$, where G is the gravitational constant [18, 19]. The mass ratio, as discussed earlier, is calculated from $\mu = m_2/(m_1 + m_2)$. The values in Table 2.1 are verified from Koon et al. and Pavlak [1, 20].

Table 2.1: Parameters in the Earth-Moon system

Quantity	Parameter	Value
Mass of Earth	m_E	5.9724×10^{24} kg
Mass of Moon	m_m	7.3460×10^{22} kg
Mass Ratio	μ	0.0122
Characteristic Length	l^*	3.8250×10^{08} m
Characteristic Mass	M	6.0459×10^{24} kg
Characteristic Time	t^*	3.7240×10^{05} s or 4.3102 days

2.3 Libration Points

The libration points are calculated in the following way: starting from the equations of motion, knowing that libration points L_1, L_2, and L_3 are collinear, the y component will always be 0. To solve for the x component, the roots of the complex equation are calculated in equations (2.3.6), (2.3.7) and (2.3.8) [17]. L_4 and L_5 are solved using geometry. L_1, L_2, and L_3 are collinear, and also unstable, while L_4 and L_5 are stable.

$$r_1^2 = (x + \mu_2)^2 + y^2 + z^2 \tag{2.3.1}$$

$$r_2^2 = (x - \mu_1)^2 + y^2 + z^2 \tag{2.3.2}$$

$$\ddot{x} - 2\dot{y} - x = -\frac{\mu_1(x+\mu_2)}{r_1^3} - \frac{\mu_2(x-\mu_1)}{r_2^3} \tag{2.3.3}$$

$$\ddot{y} + 2\dot{x} - y = -\frac{\mu_1 y}{r_1^3} - \frac{\mu_2 y}{r_2^3} \tag{2.3.4}$$

$$\ddot{z} = -\frac{\mu_1 z}{r_1^3} - \frac{\mu_2 z}{r_2^3} \tag{2.3.5}$$

Since the equilibrium points do not have a velocity or acceleration, they are set to 0, and the equations are reorganized,

$$0 = -\frac{\mu_1(x+\mu_2)}{r_1^3} - \frac{\mu_2(x-\mu_1)}{r_2^3} + x \tag{2.3.6}$$

$$0 = -\frac{\mu_1 y}{r_1^3} - \frac{\mu_2 y}{r_2^3} + y \tag{2.3.7}$$

$$0 = -\frac{\mu_1 z}{r_1^3} - \frac{\mu_2 z}{r_2^3} \tag{2.3.8}$$

Since L_1, L_2, and L_3 are all collinear, $y = 0$. Both L_4 and L_5, use geometry, so the coordinates are $[(1/2) - \mu, \sqrt{3/2}], [(1/2) - \mu, -\sqrt{3/2}]$. Table 2.2 lists the location of the libration points L_1 - L_5.

Table 2.2: Location of the libration points in the Earth-Moon system

Libration Point	x	y
L_1	0.83691800731693	0
L_2	1.15567991309474	0
L_3	-1.0050624018205	0
L_4	0.487849536707764	0.866025403784439
L_5	0.487849536707764	-0.866025403784439

2.4 Coordinate Transformation

Currently, the problem is defined in the rotating frame, so it needs to be transformed into the inertial frame rotating about the center of mass between the

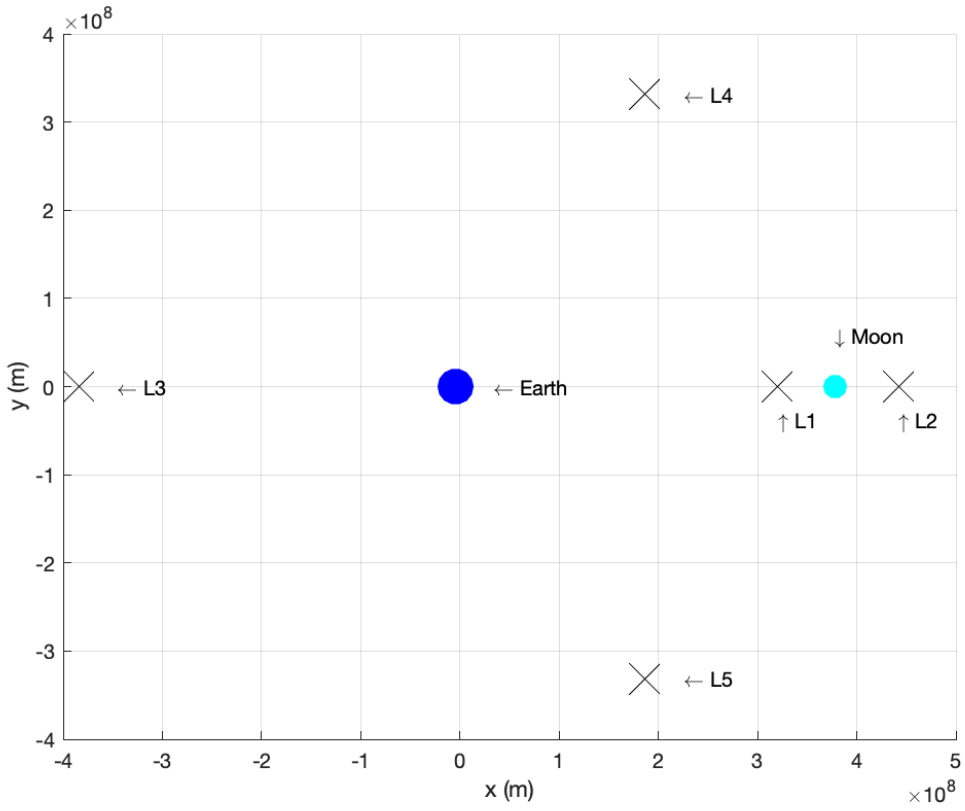

Figure 2.3.1: Location of libration points in the Earth-Moon system

two bodies to make calculations simpler.

Equation (2.4.1) is the transformation between the inertial and rotating frames using, with (X, Y, Z) as the coordinates of the rotating frame, and (x, y, z) as the coordinates of the inertial frame [1].

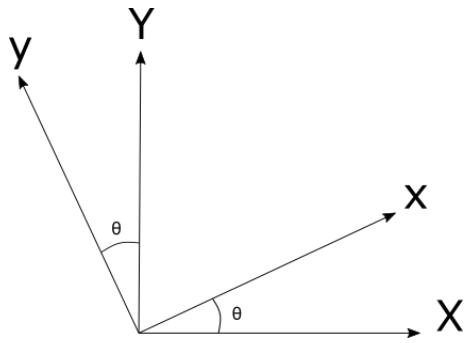

Figure 2.4.1: Rotation transformation

$$\begin{bmatrix} X \\ Y \\ Z \end{bmatrix} = A_t \begin{bmatrix} x \\ y \\ z \end{bmatrix} \tag{2.4.1}$$

where

$$A_t = \begin{bmatrix} \cos\theta & \sin\theta & 0 \\ -\sin\theta & \cos\theta & 0 \\ 0 & 0 & 1 \end{bmatrix} \tag{2.4.2}$$

The inertial frame positions for the larger primary mass is

$$(X_1, Y_1, Z_1) = (-\mu_2 \cos\theta, -\mu_2 \sin\theta, 0) \tag{2.4.3}$$

and the inertial frame position for the smaller primary mass is

$$(X_2, Y_2, Z_2) = (\mu_1 \cos\theta, \mu_1 \sin\theta, 0) \tag{2.4.4}$$

In this scenario, μ is the mass parameter, assuming that m_1 is the larger primary mass and m_2 is the smaller primary mass, $\mu = \frac{m_2}{(m_1+m_2)}$, where $\mu_1 = 1 - \mu$, and $\mu_2 = \mu$. The mass of the particle is negligible due to the minuscule mass of the particle in relation to the planetary bodies [1]. Knowing the derivation of the EOM, Equations (2.1.1) and (2.1.5) and substituting in (2.4.1), the transformation is derived to form the 6×6 transformation matrix, defined in Equation (2.4.5) [20]

$$\begin{bmatrix} X \\ Y \\ Z \\ \dot{X} \\ \dot{Y} \\ \dot{Z} \end{bmatrix} = \begin{bmatrix} \cos\theta & -\sin\theta & 0 & 0 & 0 & 0 \\ \sin\theta & \cos\theta & 0 & 0 & 0 & 0 \\ 0 & 0 & 1 & 0 & 0 & 0 \\ -\sin\theta & -\cos\theta & 0 & \cos\theta & -\sin\theta & 0 \\ \cos\theta & -\sin\theta & 0 & \sin\theta & \cos\theta & 0 \\ 0 & 0 & 1 & 0 & 0 & 1 \end{bmatrix} \begin{bmatrix} x \\ y \\ z \\ \dot{x} \\ \dot{y} \\ \dot{z} \end{bmatrix} \tag{2.4.5}$$

Given the developed transformation matrix, the pseudo-potential can be defined with the expression given in equation (2.4.6).

$$U = \frac{\mu_1}{r_1} + \frac{\mu_2}{r_2} - \frac{1}{2}(x^2 + y^2) \tag{2.4.6}$$

where (x, y, z) is the position of particle P. r_1 and r_2 are the distances to the satellite to the two planetary bodies, m_1, and m_2, respectively, defined as

$$r_1^2 = (X + \mu_2 \cos\theta)^2 + (Y + \mu_2 \sin\theta)^2 + Z^2, \tag{2.4.7}$$

$$r_2^2 = (X - \mu_1 \cos\theta)^2 + (Y - \mu_1 \sin\theta)^2 + Z^2 \tag{2.4.8}$$

with respect to the rotating frame and

$$r_1^2 = [(x + \mu_2)\cos\theta - y\sin\theta]^2 + [(x + \mu_2)\sin\theta + y\cos\theta]^2 + z^2, \tag{2.4.9}$$

$$r_2^2 = [(x - \mu_1)\cos\theta - y\sin\theta]^2 + [(x - \mu_1)\sin\theta + y\cos\theta]^2 + z^2 \tag{2.4.10}$$

with respect to the inertial frame.

2.5 Jacobi Constant

The Energy Integral and the Jacobi Constant represent the same concept and is used as a verification of the equations of motion. The energy integral is represented as $E(x, y, z, \dot{x}, \dot{y}, \dot{z}) = 1/2(\dot{x}^2 + \dot{y}^2 + \dot{z}^2) + \bar{U}(x, y, z)$, the Jacobi constant equation is represented as $C(x, y, z, \dot{x}, \dot{y}, \dot{z}) = -(\dot{x}^2 + \dot{y}^2 + \dot{z}^2) - 2\bar{U}$, and the Jacobi constant is $-2E$. Numerically, the Jacobi Constant is a relatively constant value to the degree of accuracy of the numerical integrator used to propagate the EOMs, as demonstrated in Figure 2.5.1.

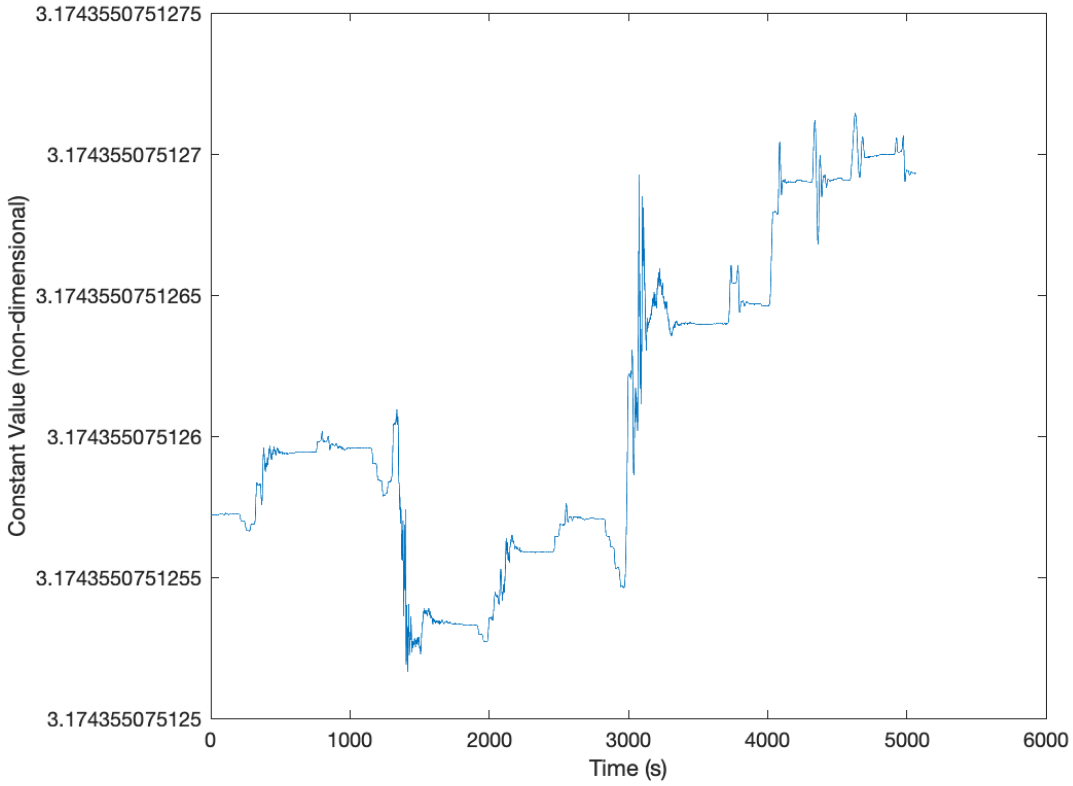

Figure 2.5.1: Jacobi constant of an orbit around L_1 in the Earth-Moon system

CHAPTER 3

GENERATING PERIODIC ORBITS

To generate the Lyapunov periodic orbits, the pseudo potential from Chapter 2 must be used to calculate the individual elements of the State Transition Matrix (STM). Once the STM is computed, a periodic orbit can be generated by using a differential corrector such as the single shooting method.

3.1 State Transition Matrix

The State Transition Matrix (STM) is a sensitivity matrix for the system, the elements measure the sensitivity of the final variation in a state to its initial perturbation [21]. The STM is denoted as $\Phi(\tau, \tau_0)$, and maps the deviations in the state vector from non-dimensional times τ_0 to τ, where non-dimensional time is defined as $\tau = \frac{t}{t^*}$ [22]. The states, $\bar{q} = [x, y, z, \dot{x}, \dot{y}, \dot{z}]^T, \dot{\bar{q}} = [\dot{x}, \dot{y}, \dot{z}, \ddot{x}, \ddot{y}, \ddot{z}]^T$, where $\partial\bar{q}$ represents a small deviation from the nominal trajectory. $\bar{f}(\bar{q} + \partial\bar{q})$ is a non-linear function, approximated using a Taylor series expansion. Neglecting the higher-order terms, expansion simplifies into: $\partial\dot{\bar{q}} = \frac{\partial\bar{f}(\bar{q})}{\partial\bar{q}}\partial\bar{q}$. The solution to the expansion is: $\partial\bar{q} = \Phi(\tau, \tau_0)\partial\bar{q_0}$, where the STM is defined as $\Phi(\tau, \tau_0) = \frac{\partial\bar{q}(t)}{\partial\bar{q}(t_0)}$, consists of partial derivatives of the state, and where $\Phi(\tau_0, \tau_0) = I$. The fundamental matrix, $A(t) = \frac{\partial\dot{\bar{q}}(t)}{\partial\bar{q}(t)}$, is evaluated along various points on a trajectory, and is generally considered not constant over the course of a trajectory [22].

For the CR3PB, A is given as:

$$A = \begin{bmatrix} 0_{3x3} & I_{3x3} \\ U_{xyz} & \Omega \end{bmatrix} \tag{3.1.1}$$

where

$$U_{xyz} = \begin{bmatrix} \frac{\partial^2 U}{\partial x \partial x} & \frac{\partial^2 U}{\partial x \partial y} & \frac{\partial^2 U}{\partial x \partial z} \\ \frac{\partial^2 U}{\partial y \partial x} & \frac{\partial^2 U}{\partial y \partial y} & \frac{\partial^2 U}{\partial y \partial z} \\ \frac{\partial^2 U}{\partial z \partial x} & \frac{\partial^2 U}{\partial z \partial y} & \frac{\partial^2 U}{\partial z \partial z} \end{bmatrix} \tag{3.1.2}$$

and

$$\Omega = \begin{bmatrix} 0 & 2 & 0 \\ -2 & 0 & 0 \\ 0 & 0 & 0 \end{bmatrix} \tag{3.1.3}$$

so that

$$A = \begin{bmatrix} 0 & 0 & 0 & 1 & 0 & 0 \\ 0 & 0 & 0 & 0 & 1 & 0 \\ 0 & 0 & 0 & 0 & 0 & 1 \\ \frac{\partial^2 U}{\partial x \partial x} & \frac{\partial^2 U}{\partial x \partial y} & \frac{\partial^2 U}{\partial x \partial z} & 0 & 2 & 0 \\ \frac{\partial^2 U}{\partial y \partial x} & \frac{\partial^2 U}{\partial y \partial y} & \frac{\partial^2 U}{\partial y \partial z} & -2 & 0 & 0 \\ \frac{\partial^2 U}{\partial z \partial x} & \frac{\partial^2 U}{\partial z \partial y} & \frac{\partial^2 U}{\partial z \partial z} & 0 & 0 & 0 \end{bmatrix} \tag{3.1.4}$$

the STM is defined as:

$$\Phi = \frac{\partial x(t)}{\partial x(t_0)} = \begin{bmatrix} \frac{\partial x}{\partial x_0} & \frac{\partial x}{\partial y_0} & \frac{\partial x}{\partial z_0} & \frac{\partial x}{\partial \dot{x}_0} & \frac{\partial x}{\partial \dot{y}_0} & \frac{\partial x}{\partial \dot{z}_0} \\ \frac{\partial y}{\partial x_0} & \frac{\partial y}{\partial y_0} & \frac{\partial y}{\partial z_0} & \frac{\partial y}{\partial \dot{x}_0} & \frac{\partial y}{\partial \dot{y}_0} & \frac{\partial y}{\partial \dot{z}_0} \\ \frac{\partial z}{\partial x_0} & \frac{\partial z}{\partial y_0} & \frac{\partial z}{\partial z_0} & \frac{\partial z}{\partial \dot{x}_0} & \frac{\partial z}{\partial \dot{y}_0} & \frac{\partial z}{\partial \dot{z}_0} \\ \frac{\partial \dot{x}}{\partial x_0} & \frac{\partial \dot{x}}{\partial y_0} & \frac{\partial \dot{x}}{\partial z_0} & \frac{\partial \dot{x}}{\partial \dot{x}_0} & \frac{\partial \dot{x}}{\partial \dot{y}_0} & \frac{\partial \dot{x}}{\partial \dot{z}_0} \\ \frac{\partial \dot{y}}{\partial x_0} & \frac{\partial \dot{y}}{\partial y_0} & \frac{\partial \dot{y}}{\partial z_0} & \frac{\partial \dot{y}}{\partial \dot{x}_0} & \frac{\partial \dot{y}}{\partial \dot{y}_0} & \frac{\partial \dot{y}}{\partial \dot{z}_0} \\ \frac{\partial \dot{z}}{\partial x_0} & \frac{\partial \dot{z}}{\partial y_0} & \frac{\partial \dot{z}}{\partial z_0} & \frac{\partial \dot{z}}{\partial \dot{x}_0} & \frac{\partial \dot{z}}{\partial \dot{y}_0} & \frac{\partial \dot{z}}{\partial \dot{z}_0} \end{bmatrix} \tag{3.1.5}$$

Substituting the general solution into the differential equations, the matrix is defined as $\dot{\Phi}(\tau, \tau_0) = A(t)\Phi(\tau, \tau_0)$. The 36 differential equations must be integrated along-side the EOMs for the CR3BP to obtain trajectory sensitivity information. The Monodromy matrix is defined as the STM over one orbit period and is useful in calculating manifolds.

3.1.1 Verifying the State Transition Matrix

To verify the STM, calculate the STM manually by starting with the initial state, then propagate it over time t, usually less than 2 days, or approximately less than 8.62 units in non-dimensional time to receive a final state. Then perturbate the initial state by 1×10^{-3} over time t, to get a final perturbed state. By taking the difference between the final state and the final perturbed state, and dividing it by the perturbation, the manually calculated STM is generated and compared to numerical integration to verify accuracy. Another way to verify the STM is by propagating it over an extremely short period of time, of approximately 0.01, and verify that the STM is close to identity.

3.2 Differential Corrector

The shooting method, also known as Newton method, adjusts the initial conditions for the EOM to turn a chaotic orbit into a periodic orbit. The shooting method propagates the trajectory for a specified time and initial conditions. The error is minimized to determine the exact velocity of the particle to maintain the orbit. The equations of motion are solved using explicit integration, and the STM provides the gradient information to 'correct' the orbit. In this project, the single shooting algorithm will be implemented to solve the boundary value problem. Figure 3.3.1, is the propagation of the EOM about L_1 before differential correction, and figure 3.3.2 is a differentially corrected Lyapunov orbit about L_1.

3.3 Periodic Orbits

There are many different families of periodic orbits around the collinear libration points, such as the Lyapunov, halo, and distant retrograde orbits. According to the Mirror Theorem from Roy and Ovenden [23], the CR3BP EOMs are invariant under the transformation of reflection across the x-axis and negative time [24, 25].

Theorem 3.3.1 (The Mirror Theorem)**.** *If n-point masses are acted upon by their mutual gravitational forces only, and at a certain epoch the radius vector from the (assumed stationary) center of mass of the system is perpendicular to every velocity vector, then the orbit of each mass after that epoch is a mirror image of its orbit prior to that epoch.*

The desired initial condition for an orbit like a Lyapunov orbit is given by

$$\vec{x_i}(\tau_0) = [x_i(\tau)\ 0\ 0\ 0\ \dot{y}_i(\tau_0)\ 0]^T \tag{3.3.1}$$

where x_i and $\dot{y}_i$ are the initial conditions for the orbit. A set of initial conditions of the form as given in equation (3.3.1) is used to calculate periodic orbits by propagating the state in the CR3BP. Using L_1 Lyapunov initial conditions provided in Grebow's thesis [22], a differential corrections method was applied to adjust the orbit to become periodic. The differential corrector was developed by implementing fzero in Matlab, searching for the exact value of $\dot{y}$ given the EOM and propagating the trajectory for one orbit period, and adjusting the calculated $\dot{y}$ for the next propagation, until the initial and final x are exactly the same. An events function is set up to determine where the trajectory crossed the y axis in the Earth-Moon frame so it will stop calculation at the point where the periodic orbit started.

Distant Retrograde Orbits (DRO) are a retrograde family of orbits that are x-axis symmetric periodic, from Theorem 3.3.1 [25]. Period-3 DRO (P3DRO) are three-revolution periodic orbits, indicating a period-tripling bifurcation occurring at the lowest Jacobi constant. The P3DROs used in this work were calculated by Dr. Capdevila as detailed in her dissertation [25]. The P3DRO is shown in Figure 3.3.3, the Earth is the blue point, and the Moon is the cyan point on the plot, as well as the libration points, indicating where the periodic orbit lies in the Earth-Moon rotating frame.

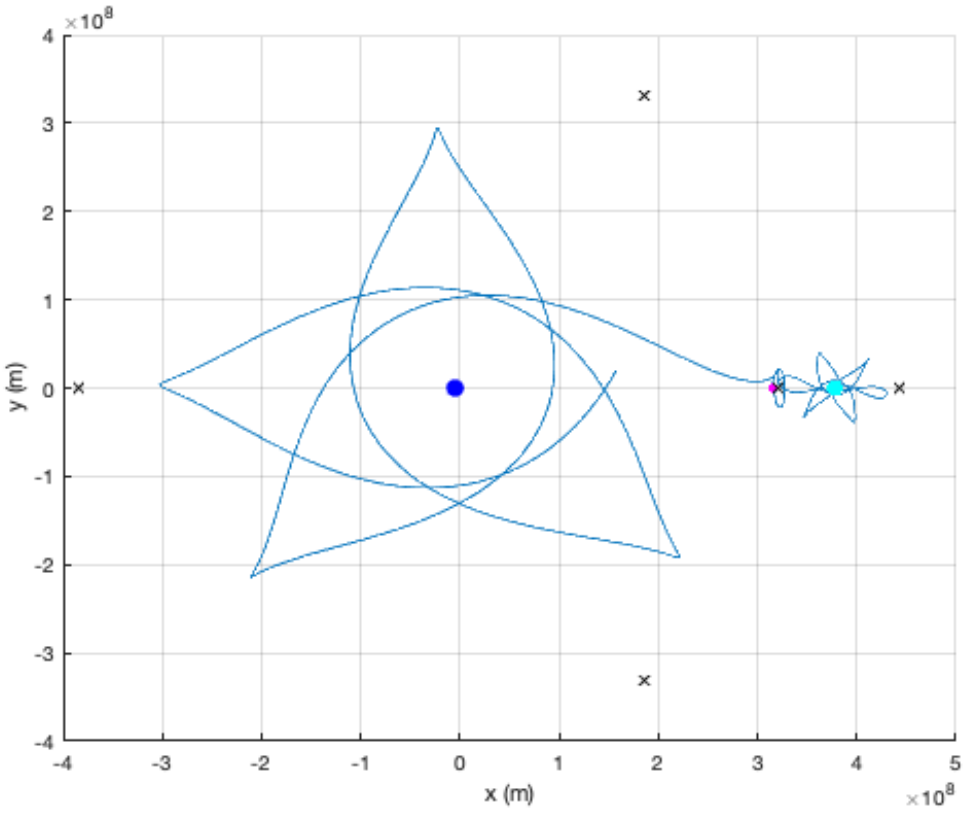

Figure 3.3.1: Initial guess for L_1 Lyapunov orbit in Earth-Moon system

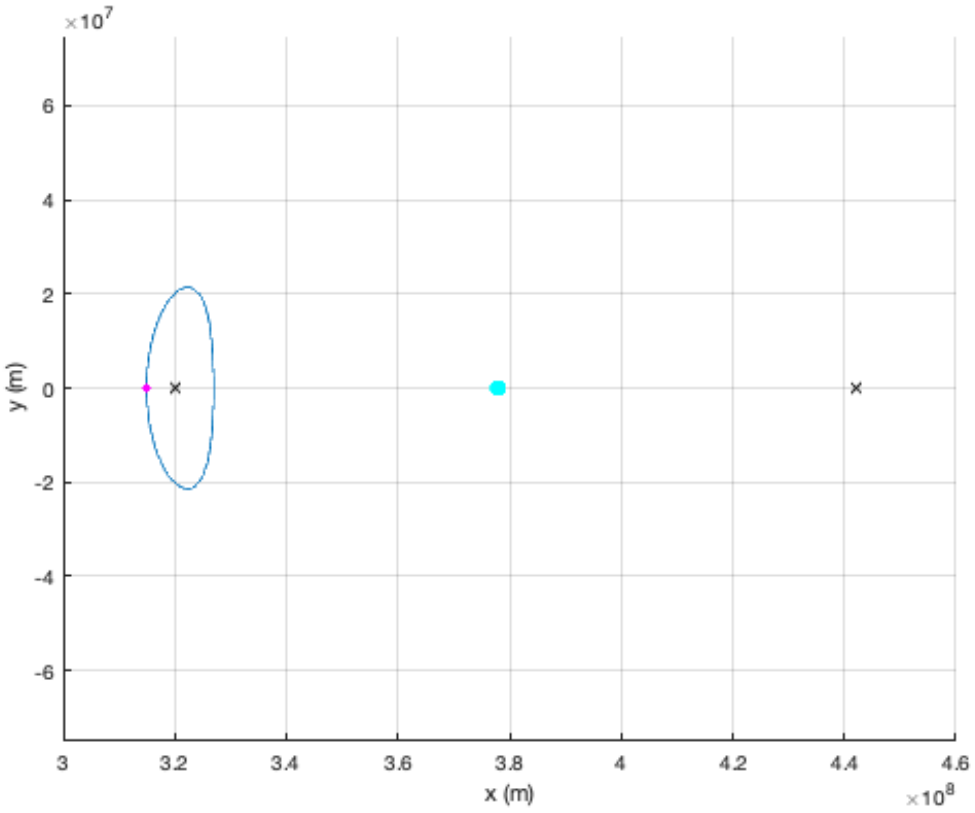

Figure 3.3.2: Lyapunov periodic orbit about L_1 in Earth-Moon system

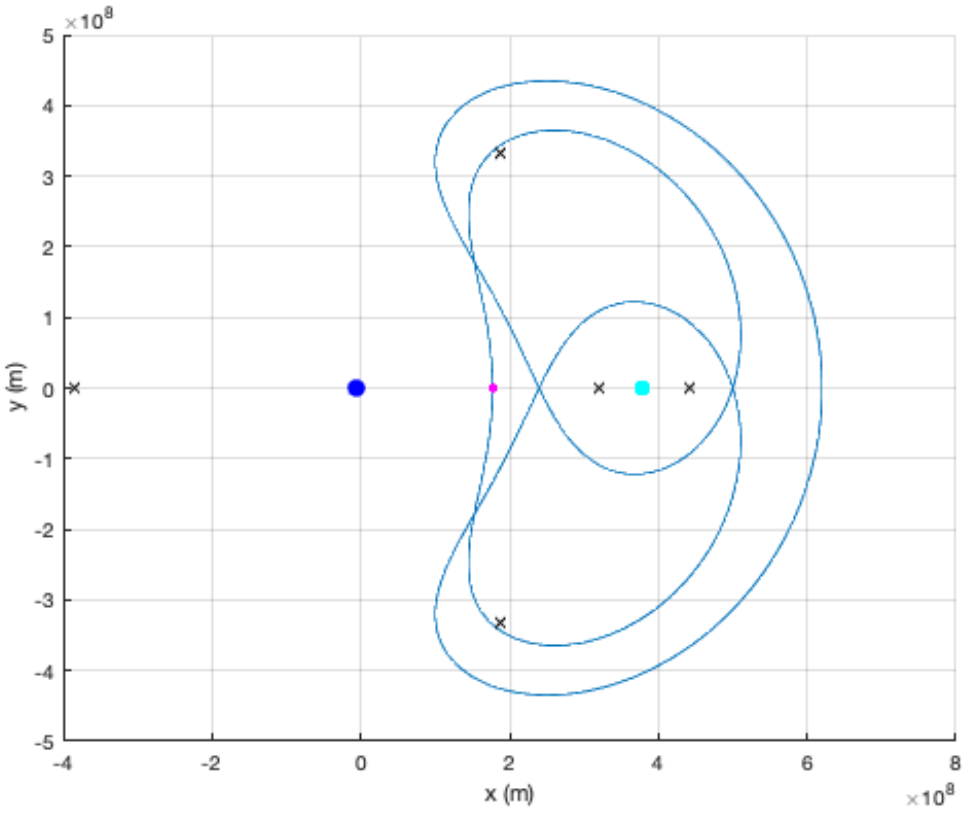

Figure 3.3.3: P3DRO periodic orbit

CHAPTER 4

INVARIANT MANIFOLDS

Invariant manifolds allow for a series of trajectories to be propagated from points on the corrected orbit. There are two sides to the manifold based on the eigenvalues calculated from the Monodromy Matrix, a stable and unstable side, both with positive and negative directions. Invariant manifold theory is based upon linear stability analysis in continuous and discrete time systems, both of which will be reviewed below [26].

4.1 Manifold Theory of fixed points

Definition of a manifold: an n-dimensional manifold $M \subset \mathbb{R}^N$ is a set for which each $x \in M$ has a neighborhood U for which there is a smooth invertible mapping (diffeomorphism) $\phi : \mathbb{R}^n \to U (n \leq N)$ [27]. Guckeheimer et al. notes smooth to mean across an infinite differential.

To start calculating the manifolds in the nonlinear system, the initial value problem is defined in Equation 4.1.1 [27]:

$$\dot{x} = f(x), x \in \mathbb{R}^n, x(0) = x_0 \tag{4.1.1}$$

where x is a member of all real n-space numbers. Starting to study the nonlinear system $\dot{x} = f(x)$, by solving for the zeros, or the 'fixed points' of the initial value problem 4.1.1.

Here, $\bar{x}$ is a fixed point, to understand the behavior near the solutions near the fixed point, equation 4.1.1 needs to be linearized to become [27]:

$$\dot{\xi} = Df(\bar{x})\xi, \xi \in \mathbb{R}^n \tag{4.1.2}$$

where $Df(\bar{x})$ is the total derivative of f at the fixed point $\bar{x}$, also defined as $Df = [\partial f_i/\partial x_j]$, the Jacobi matrix, and $x = \bar{x} + \xi, |\xi| \ll x$. Guckenheimer and Holmes provide Theorem 4.1.1 describing the stable manifold for a fixed point, [27, 9].

> **Theorem 4.1.1** (Stable Manifold Theorem for a Fixed Point)**.** *Suppose that $\dot{x} = f(x)$ has a hyperbolic fixed point $\bar{x}$. Then there exist local stable and unstable manifolds $W^s_{loc}(\bar{x})$, $W^u_{loc}(\bar{x})$, of the same dimensions n_s, n_u as those of the eigenspaces E^s, E^u of the linearized system 4.1.2, and tangent to E^s, E^u at $\bar{x}$. $W^s_{loc}(\bar{x})$, $W^s_{loc}(\bar{x})$ are as smooth as the function f.*

where $W^s_{loc}(\bar{x})$ and $W^u_{loc}(\bar{x})$ are the local invariant subspaces, or submanifolds for the system, n_s and n_u are the stable and unstable manifold dimensions respectively, and E^s and E^u are the stable and unstable subspaces for linearized systems respectively. Theorem 4.1.1 states that at any fixed point along the periodic orbit there exists a stable and unstable manifold. Stable manifolds flow towards the fixed point forward in time, while unstable manifolds flow towards the fixed point backward in time, as shown in equation 4.1.3 and equation 4.1.4 [27]. The fundamental existence-uniqueness of equation 4.1.1 ensures that distinct fixed points and their associated invariant manifolds cannot intersect.

$$W^s(\bar{x}) = \bigcup_{t \leq 0} \phi_t(W^s_{loc}(\bar{x})), \tag{4.1.3}$$

$$W^u(\bar{x}) = \bigcup_{t \geq 0} \phi_t(W^u_{loc}(\bar{x})). \tag{4.1.4}$$

Perko states in theorem 4.1.2 for nonlinear systems [28].

Theorem 4.1.2 (The Fundamental Existence-Uniqueness Theorem)**.** *Let E be an open subset of $\mathbb{R}^n$ containing x_0 and assume that $f \in C^1(E)$. Then there exists an $a > 0$ such that the initial value problem*

$$\dot{x} = f(x) \tag{4.1.5}$$

$$x(0) = x_0 \tag{4.1.6}$$

has a unique solution $x(t)$ on the interval $[-a, a]$.

where E is an open subset of $\mathbb{R}^n$. Perko went into further detail of the proof of the fundamental existance-uniqueness theorem in his book [28].

Guckenheimer and Holmes provide Theorem 4.1.3 describing the stable manifold for a fixed point where $W^s_{loc}(\bar{x})$ and $W^u_{loc}(\bar{x})$ are the local invariant subspaces, or submanifolds for the system, n_s and n_u are the stable and unstable manifold dimensions respectively, and E^s and E^u are the stable and unstable subspaces for linearized systems respectively [27].

Theorem 4.1.3 (Stable Manifold Theorem for a Fixed Point)**.** *Let G: $\mathbb{R}^n \to \mathbb{R}^n$ be a (C^1) diffeomorphism with a hyperbolic fixed point $\bar{x}$. Then there are local stable and unstable manifolds $W^s_{loc}(\bar{x})$, $W^u_{loc}(\bar{x})$, tangent to the eigenspaces $E^s_{\bar{x}}$, $E^u_{\bar{x}}$ of $DG(\bar{x})$ at $\bar{x}$ and of corresponding dimensions. $W^s_{loc}(\bar{x})$, $W^u_{loc}(\bar{x})$ are as smooth as the map G.*

4.1.1 Eigenvalues

Definition of eigenvector: An eigenvector v of an $n \times n$ matrix A is a nonzero vector whch satisfies $Av = \lambda v$ or $(A - \lambda I)v = 0$ for some $\lambda \in \mathbb{C}$; λ is the eigenvalue of v, where $\mathbb{C}$ are complex numbers [27]. Associated with the monodromy matrix for a particular periodic orbit in the CR3BP, there are a set of six eigenvalues, two are close to zero, two are equal to each other, and the ones without complex parts are the ones used to calculate the manifolds. The position of the eigenvalues determines the correct set of eigenvectors to use in manifold calculation.

4.2 Methodology to Calculate Invariant Manifolds

Starting with the differentially corrected periodic orbit, the number of points along the periodic orbit to start trajectories is determined. It is best to start with a relatively small number of cases such as 20 when generating a series of trajectories on the manifolds. Next, the fixed points and their respective times along the periodic orbit are selected, and stored in a variable for future reference. Next the STM is recalculated for each fixed point for approximately 2 orbit periods, and the corresponding eigenvalues and eigenvectors are calculated. This processes of calculating manifolds is demonstrated in the flowchart shown in Figure 4.2.1.

Using the eigenvalues and corresponding fixed points, the initial conditions used to propagate in the CRTBP are recalculated depending on the manifolds generated, such as stable or unstable, and the direction of the manifold, whether it is positive or negative. The eigenvalues selected correspond to the set of eigenvectors used to determine the new initial conditions for the specific manifold. The general equation for the initial conditions that will be propagated in the CR3BP is noted in Equation 4.2.1:

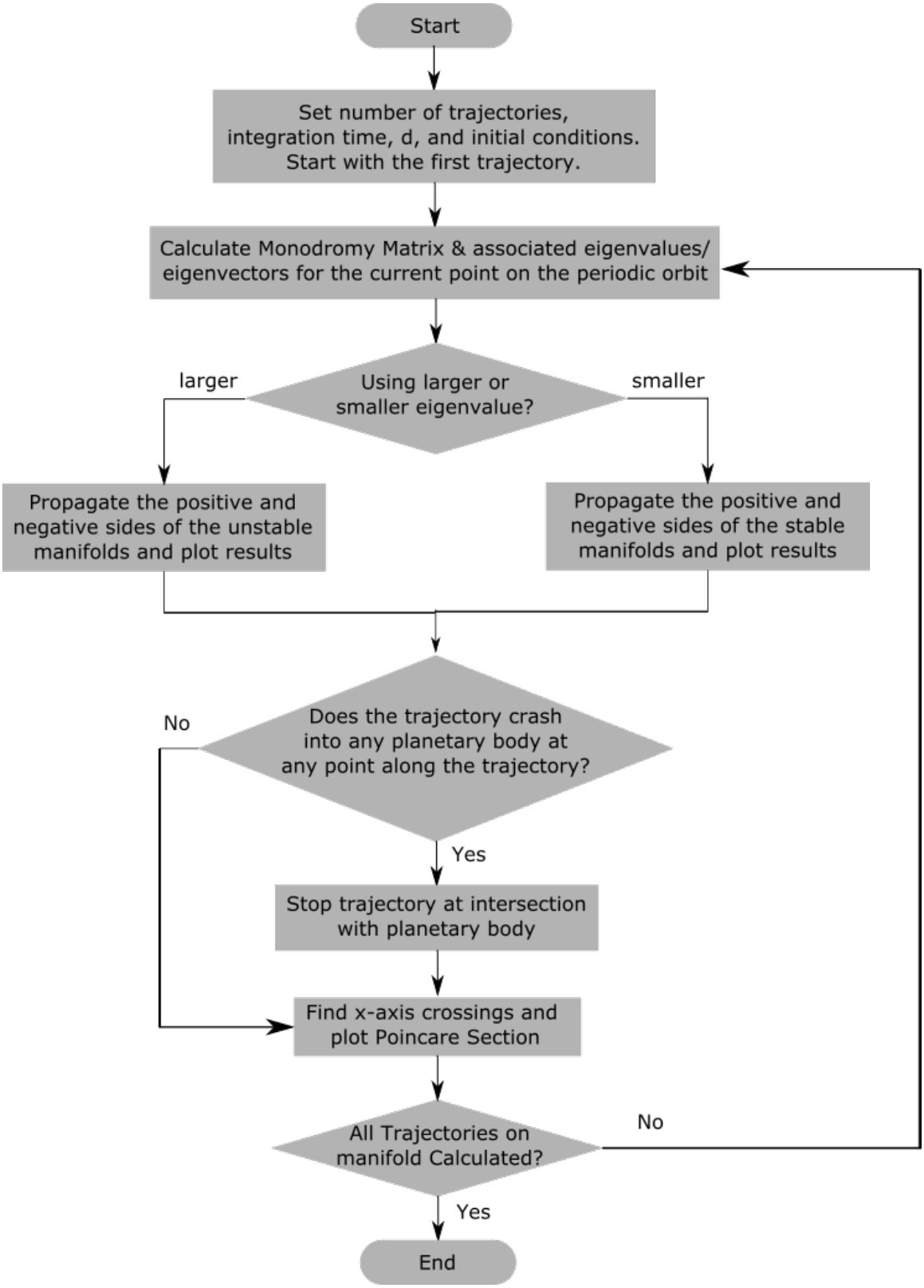

Figure 4.2.1: Flowchart for detecting crashing manifold trajectories

$$\vec{x} \pm d\frac{\vec{v}}{\|\vec{v}\|} \tag{4.2.1}$$

$$\|\vec{v}\| = \|[xyz]^T\| \tag{4.2.2}$$

Where $\vec{x} = [xyz\dot{x}\dot{y}\dot{z}]^T$ are the fixed points along the periodic orbit, vector $\vec{v}$ is the eigenvector of the monodromy matrix associated with a specific fixed point along the periodic orbit. The eigenvectors are a 6×1 vector that are corresponding to the selected eigenvalue λ, and d is the distance away from the fixed point, here set to 1×10^{-5} non-dimensional length units. The largest and smallest magnitude eigenvalues and associated eigenvectors must be identified for each fixed point along the periodic orbit.

4.2.1 Calculating the Stable Manifolds

Since stable manifolds flow towards the orbit in forwards time, they are computed in backwards time and are associated with the eigenvalue of the smallest magnitude. To create the initial conditions that will be propagated, the smallest magnitude eigenvalue is used to determine the corresponding eigenvector, which is added to the initial starting point along the periodic orbit. Depending on the direction of the trajectory, Equation 4.2.1 is either added for the positive direction, or subtracted for the negative direction, as exemplified in Figures 4.2.2 and 4.2.3, showing stable manifold trajectories associated with a Lyapunov and a P3DRO, respectively. The green trajectories are positive meaning the eigenvectors were added to the initial points, and the blue trajectories are negative, meaning the eigenvectors were subtracted from the initial points. Figures 4.2.2 and 4.2.3 show a projection of the manifold trajectories as they appear in the x-y plane. However the

trajectories exist in a 6-dimensional space, where they do not intersect with each other, as explained in Theorem 4.1.2.

4.2.2 Calculating the Unstable Manifolds

The unstable manifolds are computed forwards in time and are associated with the larger magnitude eigenvalue. Similar to the stable manifold, the initial conditions that will be propagated use the eigenvector associated with the larger magnitude eigenvalue. Depending on the direction of the trajectory, Equation 4.2.1 is either added for the positive direction, or subtracted for the negative direction, as exemplified in Figure 4.2.4, the stable manifolds around the Lyapunov orbit, and in Figure 4.2.5. In this case, the red trajectories are positive, and the magenta trajectories are negative. Forwards in time, the manifold trajectories flow away from their respective periodic orbits, making them the best viable trajectories leading to Mars.

4.2.3 Verifying the manifolds

To verify the computation of manifold trajectories, it is insightful to propagate the stable manifolds forwards in time, and the unstable manifolds backwards in time, that is opposite to how manifolds are calculated. When propagating the unstable manifolds backwards in time, it is expected that the trajectory will approach the periodic orbit. Propagating the unstable manifold backwards in time by approximately two orbit periods and verifying that it converges to the periodic orbit is how the manifolds are verified to be calculated correctly, as shown in Figure 4.2.6

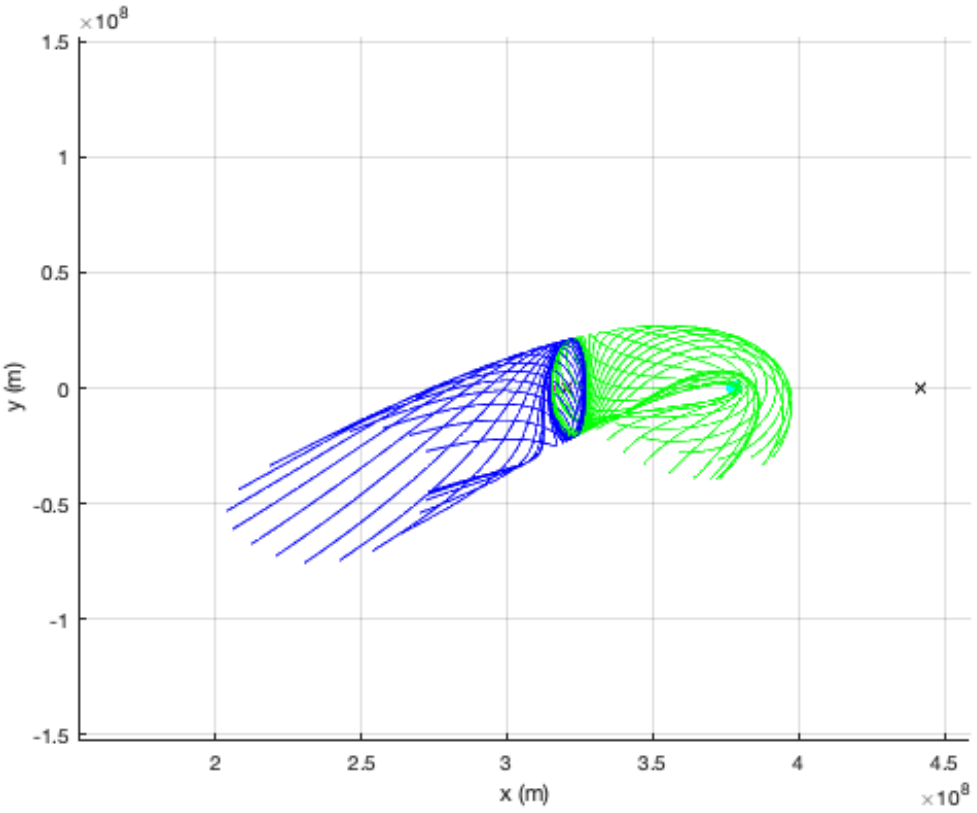

Figure 4.2.2: Stable Lyapunov manifolds

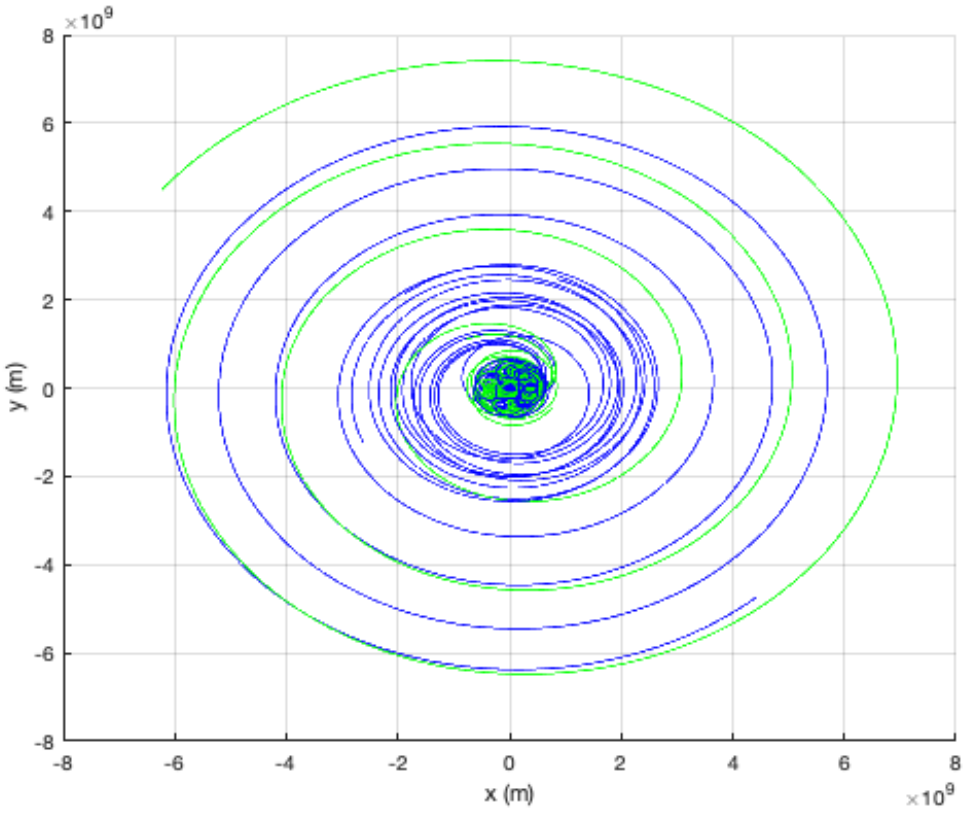

Figure 4.2.3: Stable P3DRO manifolds

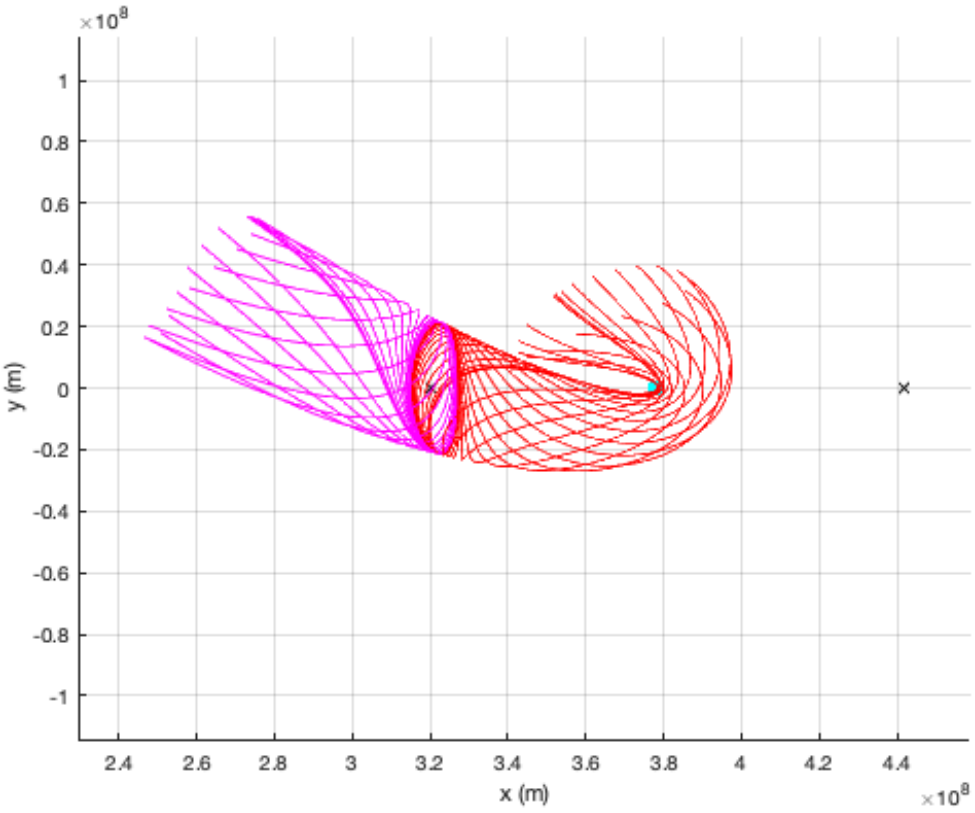

Figure 4.2.4: Unstable Lyapunov manifolds

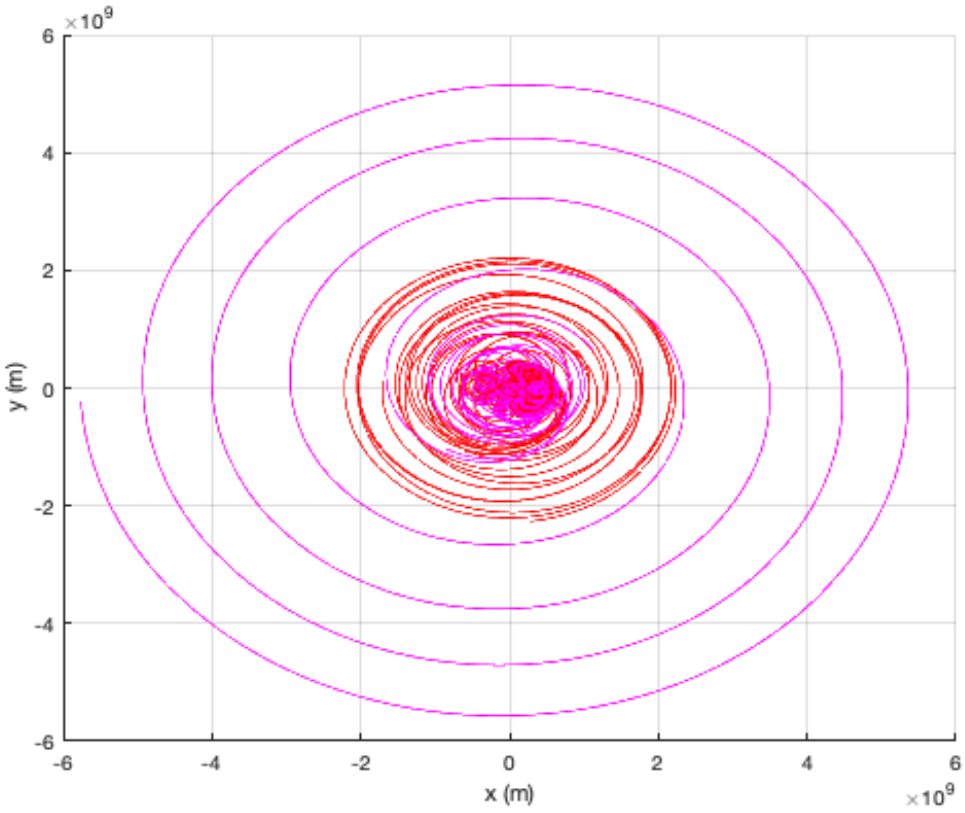

Figure 4.2.5: Unstable P3DRO manifolds

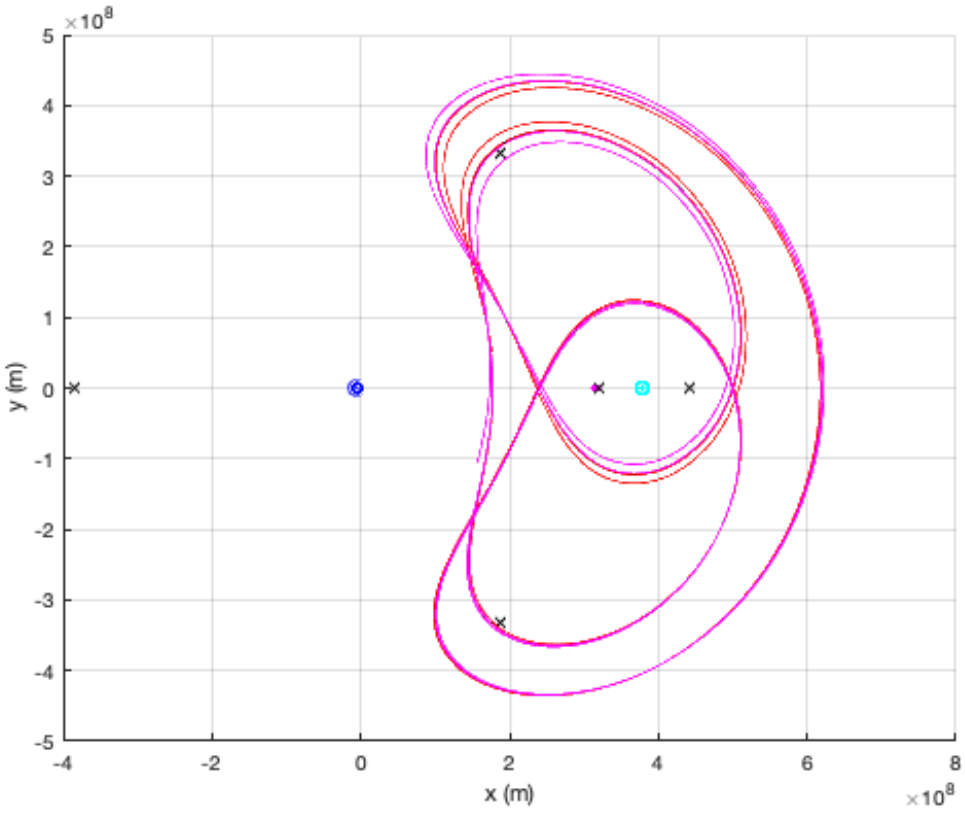

Figure 4.2.6: Verifying unstable manifolds converge into periodic orbit

4.2.4 Finding a feasible trajectory

To find a feasible trajectory, trajectories that intersect with the planetary bodies must first be eliminated. In Figures 4.2.7 and 4.2.8, the trajectories are terminated at the surface of the planetary bodies they intersect. Thus, unfeasible trajectories are eliminated before further evaluation. Figures 4.2.7 and 4.2.8 show 100 potential trajectories for each direction and their collisions with planetary bodies, if they intersect with the surface of the planet. The cyan circle represents the surface of the Moon, while the blue circle represents the surface of the Earth. While it is known that the atmosphere can impact the geometry of trajectories, is it not accounted for in this investigation.

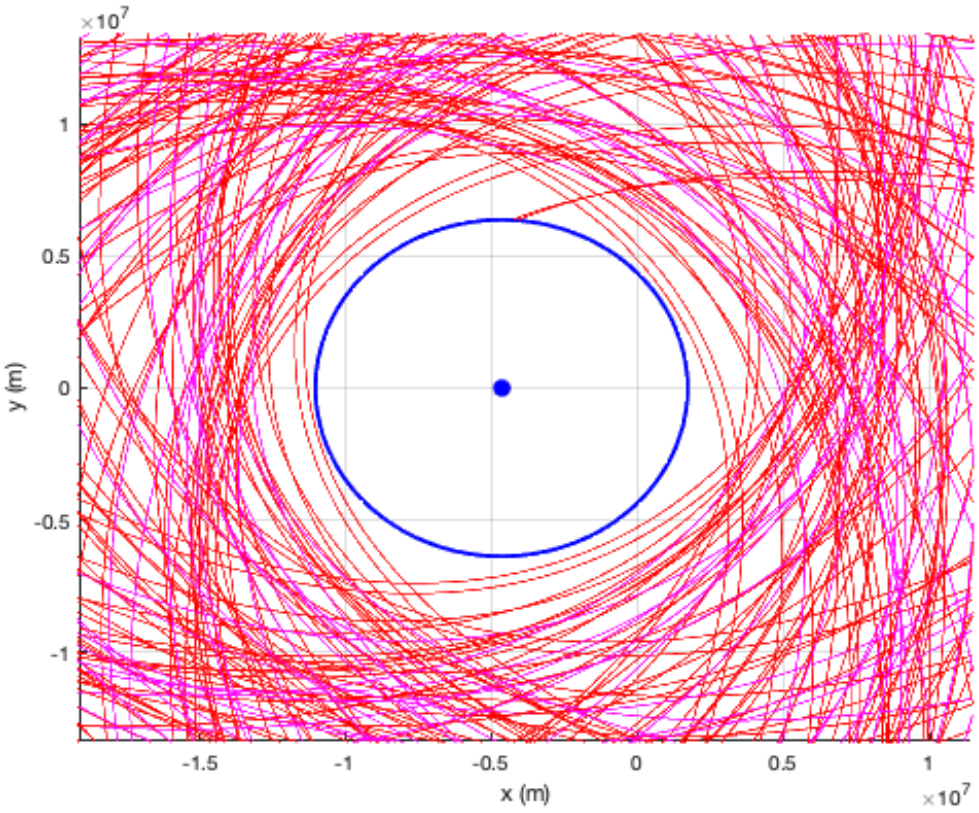

Figure 4.2.7: Trajectories intersecting with the Earth

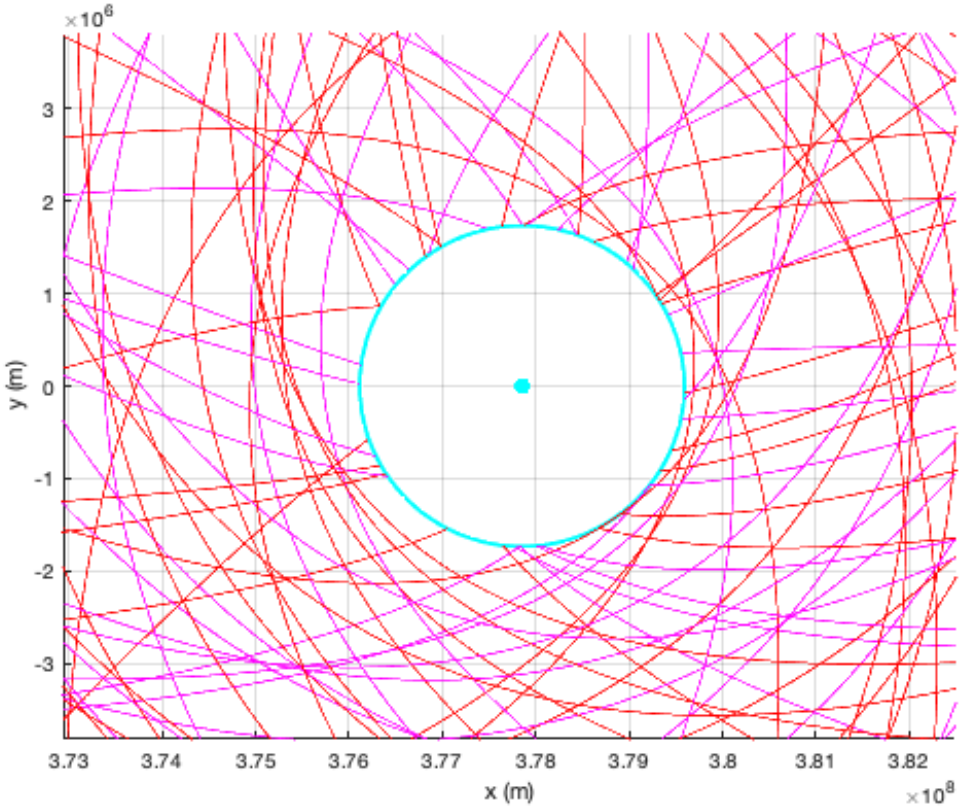

Figure 4.2.8: Trajectories intersecting with the Moon

CHAPTER 5

ANALYSIS OF TRAJECTORIES AND RESULTS

Only the unstable manifolds can become candidate trajectories because they naturally progress away from the periodic orbit. To find a suitable candidate trajectory, the steps in Chapter 4 are implemented, 100 candidate trajectories are calculated and a candidate trajectory leaving the Earth-Moon system is found. After the viable trajectories are determined, one trajectory is further evaluated for its potential to reach Martian orbit.

5.1 Viable Orbits

A viable orbit is identified as one associated with no collisions to a planetary body, and if the manifold can extend out to Martial orbit. As shown in Figure 5.1.1, out of 100 unstable trajectories in the positive direction and 100 unstable trajectories in the negative direction, a potential 63 positive (red) viable orbits are available, while a potential 71 negative (magenta) orbits exist to reach Mars' orbit, meaning they do not intersect with the Earth and Moon for a timeframe of 150 periodic orbit periods, or approximately 2,594.6 days. Of the 134 possible viable trajectories, only some have the capacity to extend out far enough to reach Mars' orbit. The Earth to Mars distance is between 203.7719 and 982.1283 nondimensional Earth-Moon units of distance, that is, between 78,327,500 and 377,518,500 km [29]. Figure 5.1.1 demonstrates that a trajectory can reach Mars' orbit, where the black trajectory is a representation of the furthest distance the

viable trajectory would need to reach to intersect Mars' orbit. The Sun's orbit around Earth is accurately depicted in yellow for reference.

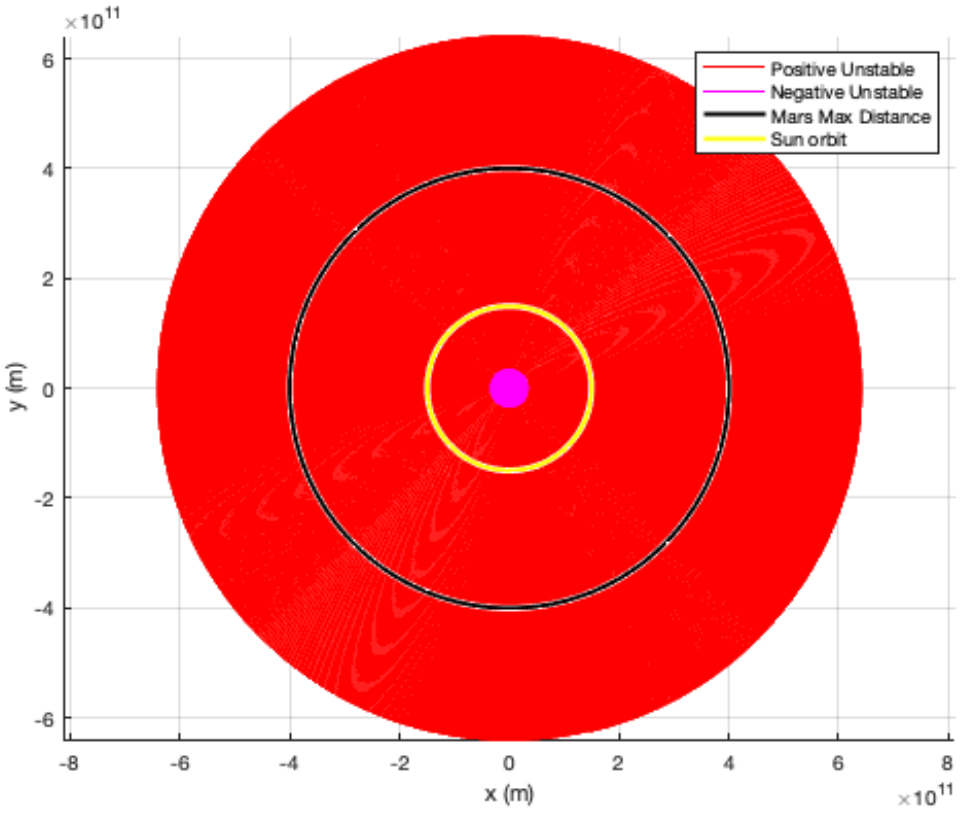

Figure 5.1.1: Potential viable trajectory to Mars in the rotating frame

CHAPTER 6

CONCLUSION

In conclusion, the primary goal of determining the possibility of reaching Mars using a P3DRO has been achieved. Initial goals involved contributing to the IPS [6], and add to the current literature exploring a way to navigate the solar system with the minimum amounts of ΔV. An Earth-Moon CR3BP was defined through the calculation of the Earth-Moon characteristic quantities, simulated, and verified through numerical propagation of the equations of motion. By generating and verifying the state transition matrix, periodic orbits were created through differential corrections to ensure periodicity. The invariant manifolds were calculated from the periodic orbits and verified to ensure the trajectories produced are indeed on the manifold associated with their respective periodic orbit. Lastly, several viable trajectories towards Mars' were identified, and it is now confirmed that a trajectory originating from a P3DRO manifold can reach Mars.

6.1 Future Work

Future work involves looking at a higher fidelity model of the Martian orbit transformed into the Earth-Moon rotating reference frame and/or the transformation of manifold trajectories into Sun-centered inertial frame to more accurately assess if manifold trajectories reach the Martian system. Once the transformations are completed, the approach velocity of each trajectory can be compared and determine how large of a ΔV will be required for a rendezvous within

the Martian system.

REFERENCES

[1] W. S. Koon, M. W. Lo, J. E. Marsden, and S. D. Ross, *Dynamical Systems, the Three-Body Problem and Space Mission Design*. 1.2 ed., April 2011.

[2] F. Topputo, M. Vasile, and F. Bernelli-Zazzera, "Low energy interplanerary transfers exploiting invariant manifolds of the restricted three-body problem," *Journal of the Astronautical Sciences*, vol. 53, pp. 353–372, October - December 2005.

[3] A. D. Cox, K. C. Howell, and D. C. Folta, "Trajectory design leveraging low-thrust, multi-body equilibria and their manifolds," August 2018.

[4] J. Heiligers, G. Mingotti, and C. McInnes, "Optimisation of solar sail interplanetary heteroclinic connections," March 2014.

[5] M. Varquero and K. C. Howell, "Leveraging resonant-orbit manifolds to design transfers between libration-point orbits," *Journal of Guidance Control and Dynamics*, vol. 37, July - August 2014.

[6] M. W. Lo, "The interplanetary superhighway and the origins program," *IEEE*, 2002.

[7] *BepiColumbo Gravitational Capture and the Elliptic Restricted Three-Body Problem*, 2008.

[8] C. Finocchietti, P. Pergola, and M. Andrenucci, "Venus transfer design by combining invariant manifolds and low-thrust arcs," *Acta Astronautica*, vol. 94, no. 1, pp. 351 – 362, 2014.

[9] M. Kakoi, *Design of Transfer from Earth-Moon L1/L2 Libration Point Orbits to a Destination Object*. PhD thesis, Purdue University, 2015.

[10] F. Topputo and E. Belbruno, "Earth–mars transfers with ballistic capture," *Celestial Mechanics and Dynamical Astronomy*, vol. 121, no. 4, pp. 329–346, 2015.

[11] E. A. Belbruno and J. K. Miller, "Sun-perturbed earth-to-moon transfers with ballistic capture," *Journal of Guidance Control and Dynamics*, vol. 16, pp. 770–775, July-August 1993.

[12] E. Barrabés, G. Gomez, J. Mondelo, and M. Ollé, "Pseudo-heteroclinic connections between bicircular restricted four-body problems," *Monthly Notices of the Royal Astronomical Society*, vol. 462, 07 2016.

[13] N. Bosanac, J. Marsden, A. Moore, and S. Campagnola, "Titan trajectory design using invariant manifolds and resonant gravity assists," vol. 136, 01 2010.

[14] P. Pergola, K. Geurts, C. Casaregola, and M. Andrenucci, "Power constrained uranus transfer and moons tour by three body invariant manifolds and electric propulsion," 01 2008.

[15] T. Stuchi, T. Yokoyama, A. Corrêa, R. Solórzano, D. Sanchez, S. Winter, and O. Winter, "Dynamics of a spacecraft and normalization around lagrangian points in the neptune–triton system," *Advances in Space Research*, vol. 42, no. 10, pp. 1715 – 1722, 2008.

[16] Y. Liang, M. Xu, and S. Xu, "Low-energy weak stability boundary transfers to pluto's moons: Preliminary trajectory design via triangular libration point," *Acta Astronautica*, vol. 156, pp. 219 – 233, 2019.

[17] V. Szebehely, *Theory of Orbits; The Restricted Problem of Three Bodies*. ll Fifth Avenue New York 111 Fifth Avenue, New York, New York 10003: Academic Press Inc., 1967.

[18] National Aeronautics and Space Administration, "Distance to the moon," October 2009.

[19] M. Wieczorek, B. Jolliff, A. Khan, M. Pritchard, B. Weiss, J. Williams, L. Hood, K. Righter, C. Neal, C. Shearer, I. S. Mccallum, S. Tompkins, B. R. Hawke, C. Peterson, J. J. Gillis, and B. Bussey, "The constitution and structure of the lunar interior," *Reviews in Mineralogy & Geochemistry*, vol. 60, pp. 221–364, 2006.

[20] T. A. Pavlak, *Trajectory Design and Orbit Maintenance Strategies in Multi-Body Dynamical Regimes*. PhD thesis, Purdue University, 2013.

[21] A. F. Haapala, "Trajectory design using periapse maps and invariant manifolds," Master's thesis, Purdue University, 2010.

[22] D. J. Grebow, "Generating periodic orbits in the circular restricted three-body problem with applications to lunar south pole coverage," Master's thesis, Purdue University, 2006.

[23] A. E. Roy and M. W. Ovenden, "On the occurrence of the commensurable mean motions in the solar system: The mirror theorem," *Monthly Notices of the Royal Astronomical Society*, vol. 115, pp. 296–309, June 1955.

[24] L. R. Irrgang, "Investication of transfer trajectories to and from the equilateral libration points l4 and l5 in the earth-moon system," Master's thesis, Purdue University, August 2008.

[25] L. R. Capdevila, *A Transfer Network Linking Earth, Moon, and the Triangular Libration Point Revions in the Earth-Moon System*. PhD thesis, Purdue University, May 2016.

[26] B. T. Barden, "Using stable manifolds to generate transfers in the circular restricted problem of three bodies," Master's thesis, Purdue University, December 1994.

[27] J. Guckenheimer and H. Philip, *Nonlinear Oscillations, Dynamical Systems, and Bifurcations of Vector Fields*, vol. 42 of *Applied Mathematical Sciences*. Springer Science + Business Media New York, 1 ed., 1983.

[28] L. Perko, *Differential Equations and Dynamical Systems*, vol. 7 of *Texts in Applied Mathematics*. Springer-Verlag, 1 ed., 1991.

[29] National Aeronautics and Space Administration, "Mars the red planet," March 2021.